SEVEN
EDITORA
2026

ANALYSIS OF THE BAR PROBLEM UNDER NORMAL FORCE VIA UNCONVENTIONAL FORMULATIONS OF THE FINITE ELEMENT METHOD

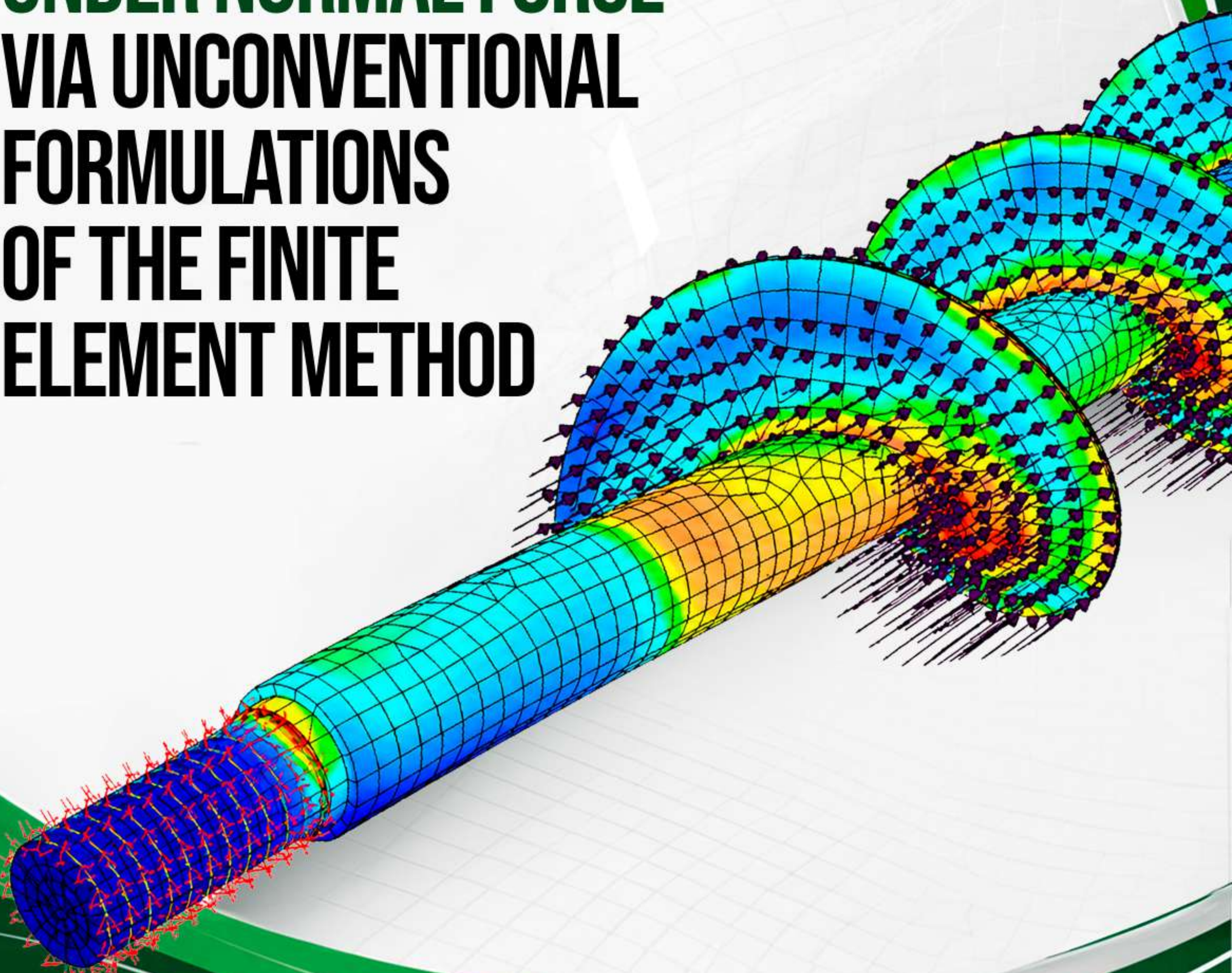

JOSÉ VIEIRA DE MELO NETO, LUIS ARMANDO PICCINO NAVARRO, EDSON DA COSTA EDUARDO, STEFAN HASS, RAFAELA RODRIGUES GOMES, WESLEY GÓIS

Dados Internacionais de Catalogação na Publicação (CIP)
(Câmara Brasileira do Livro, SP, Brasil)

A532

Analysis of the Bar Problem Under Normal Force via Unconventional Formulations of the Finite Element Method [recurso eletrônico] / José Vieira de Melo Neto ... [et al.]. – São José dos Pinhais, PR: Editora Seven, 2026.

Dados eletrônicos (1 PDF).

Inclui bibliografia.

ISBN 978-65-6109-439-9

1. Engenharia. 2. Simulação. I. Melo Neto, José Vieira de. II. Navarro, Luis Armando Piccino. III. Eduardo, Edson da Costa. IV. Hass, Stefan. V. Título.

CDU 63

Bruna Heller - Bibliotecária - CRB10/2348

Índices para catálogo sistemático:

1 Agricultura 63

DOI: 10.56238/livrosindi2026109-001

Seven Publications Company
CNPJ: 43.789.355/0001-14
editora@sevenevents.com.br
São José dos Pinhais/PR

THE AUTHORS

José Vieira de Melo Neto
Federal University of ABC – UFABC
Master's degree in Mechanical Engineering
joseneto86@hotmail.com
https://orcid.org/0009-0000-5993-050X

Luis Armando Piccino Navarro
Federal University of ABC – UFABC
Master's degree in Mechanical Engineering
luispiccino@gmail.com
https://orcid.org/0009-0001-4974-3089

Edson da Costa Eduardo
Federal University of ABC – UFABC
Master's degree in Mechanical Engineering
ededu84@gmail.com
https://orcid.org/0009-0003-3850-9451

Stefan Hass
Master's degree in Mechanical Engineering
University of Applied Sciences Offenburg
Department for Mechanical and Process Engineering
Badstr. 24, 77652 Offenburg, Germany
haas.stef26@googlemail.com
https://orcid.org/0009-0002-6261-6356

Rafaela Rodrigues Gomes
Federal University of ABC – UFABC
Aerospace Engineer
rafaelarodriguesgomes1@gmail.com
https://orcid.org/0009-0000-3682-339X

Wesley Góis
Federal University of ABC – Engineering, Modeling and Applied Social Sciences Center - Aerospace Engineering, Alameda da Universidade, 09606-070, São Bernardo do Campo, São Paulo, Brazil
wesley.gois@ufabc.edu.br
https://orcid.org/0000-0003-3088-6394

ABSTRACT

This work highlights the application of unconventional formulations of the Finite Element Method (FEM) to the analysis of the classical one-dimensional Structural Mechanics problem of a bar subjected to axial loading. Specifically, the Hybrid-Mixed Stress Formulation (HMSF), the Generalized Finite Element Method (GFEM), the Stable Generalized Finite Element Method (SGFEM), and the application of GFEM and SGFEM within the HMSF framework are employed in the numerical simulation of this problem using MatLab® and SMath®. The main objective of this article is to present, in a didactic manner, the mathematical and numerical foundations of each of the five unconventional FEM formulations considered, together with a set of routines developed in MatLab® and SMath®. Through this simple application, the reader is expected to understand the construction of the approximation bases associated with the field variables involved in the weak formulation of the problem, the explicit matrix structure of the resulting discrete system of equations, and the principles and methodology of nodal enrichment. Finally, this work also seeks to enhance the understanding of the limitations and potential of these unconventional FEM formulations in the analysis of Structural Mechanics problems.

Keywords: Finite Element Method, Generalized Finite Element Method, Stable Generalized Finite Element Method, Hybrid-Mixed Stress Formulation, Bar Problem under Normal Force.

SUMMARY

INTRODUCTION

Since the emergence of the Finite Element Method (FEM) for the analysis of Structural Mechanics problems in 1956, several unconventional FEM formulations have been developed to overcome limitations associated with the classical displacement-based formulation, particularly in the simulation of crack propagation problems. Specifically, this work highlights the unconventional FEM formulations known as the Generalized Finite Element Method (GFEM), the Stable Generalized Finite Element Method (SGFEM), the Hybrid-Mixed Stress Formulation (HMSF), the application of the Generalized Finite Element Method within the HMSF framework (HMSF-GFEM), and the application of the Stable Generalized Finite Element Method within the HMSF framework (HMSF-SGFEM), with the aim of applying them to the solution of the one-dimensional problem of a bar subjected to axial loading.

In most publications addressing unconventional FEM formulations, particularly for the analysis of linear elasticity problems, one does not find a simple and step-by-step presentation that clearly explains how the approximation and enrichment functions are defined, how the weak formulation of the problem is derived, issues related to the solution procedure for the resulting system of discrete equations, and the structure of the computational code employed in the simulations. Furthermore, the evaluation of the computational implementation itself is often difficult, since the source codes are generally not made available in scientific publications or are designed for the analysis of two- or three-dimensional problems using low-level programming languages, such as Python, Fortran, and C, resulting in extensive and highly complex codes.

Typically, scientific works present the elasticity equations in two or three dimensions, expressed in weak form using tensor notation, together with a compact matrix representation of the implementation of the unconventional FEM formulations. In this context, the objective of the present work is to provide a didactic, step-by-step approach to the presentation of the fundamentals of each unconventional FEM formulation applied to the numerical solution of the one-dimensional bar problem. The aim is to clearly explain the complete structure of these unconventional numerical methods, including their particularities and limitations, with the support of MatLab® and SMath® tools.

Specifically, the GFEM and SGFEM are numerical approaches derived essentially from the combination of advantageous features of the conventional displacement-based

FEM and Meshless Methods, as discussed by authors in the literature, including Babuška, Caloz and Osborn (1994), Duarte and Oden (1996), Babuška and Melenk (1997), Oden, Duarte and Zienkiewicz (1998), Duarte, Babuška and Oden (2000), Strouboulis, Babuška and Copps (2000), and Gupta et al. (2013).

In the GFEM and SGFEM, a cover mesh is employed to define support clouds within which the shape functions of the classical FEM are used as a Partition of Unity (PU). These shape functions can then be enriched within each cloud through their multiplication by functions of interest, whether polynomial or non-polynomial. As a result, the enrichment procedure acquires a nodal character, as discussed by Duarte, Babuška and Oden (2000) and Gupta et al. (2013).

In summary, nodal enrichment can be defined as the expansion of the approximation bases involved in the formulation without the need to introduce additional nodal points into the domain. It is important to note that there are slight differences between the nodal enrichment methodologies employed in the GFEM and SGFEM, as discussed by Gupta et al. (2013). Consequently, this strategy differs from the *p*-adaptive process of the classical FEM, which, for certain classes of finite elements, requires the insertion of additional nodal points within the elements in order to increase the interpolation degree, Duarte and Oden (1996).

The Hybrid-Mixed Stress Formulation (HMSF), as presented by DE Freitas, DE Almeida, and Pereira (1996), Góis (2009), and Góis and Proença (2012), differs from the FEM, GFEM, and SGFEM formulations in that it does not approximate only the displacement field directly. Instead, it involves the simultaneous approximation of three fields: stresses and displacements within the domain, and displacements along the problem boundary. Consequently, in the HMSF, two covering meshes are required for the discretization of the problem into finite elements: one associated with the domain and another associated with the boundary.

In Góis (2009) and Góis and Proença (2012), the application of the GFEM nodal enrichment technique within the HMSF framework is proposed, giving rise to the HMSF-GFEM formulation. Subsequently, Neto, Góis, and Lins (2022) presented the application of the SGFEM nodal enrichment strategy within the HMSF framework, resulting in the HMSF-SGFEM formulation.

It is expected that the numerical solution of the bar problem subjected to axial loading, using these unconventional FEM formulations through MatLab® and SMath®, will provide a clearer understanding of the application of these numerical methods in the context of Structural Mechanics problems.

The remainder of this text is organized as follows. Section 2 presents the bar problem subjected to axial loading in its so-called strong form, together with the fundamental relationships associated with the HMSF, GFEM, SGFEM, HMSF-GFEM, and HMSF-SGFEM formulations. Section 3 presents the numerical simulations developed in this work. Finally, Section 4 summarizes the main conclusions of the study.

HYBRID-MIXED STRESS FORMULATION APPLIED TO ONE-DIMENSIONAL ELASTICITY

2.1 HYBRID-MIXED STRESS FORMULATION FOR A ONE-DIMENSIONAL (1D) ELASTICITY PROBLEM

The objective of this chapter is to present the application of the HMSF to a one-dimensional problem consisting of a bar subjected to axial loading. First, a brief description of the proposed problem and the development of its strong form are presented. Subsequently, the HMSF is defined through the Weighted Residuals Method (WRM) and applied to the numerical simulation of the problem.

The problem of a bar subjected to axial loading consists of a prismatic bar with constant cross-sectional area A, L ($L >> A$), subjected to a uniformly distributed load q (force per unit length) over the interval $0 \leq x \leq L$, that is, throughout the domain. In addition, a concentrated force P is applied at the boundary x = L, where both q and P act normal to the cross-sectional area A. Small displacements are assumed, equilibrium is considered in the initial configuration of the system, and the bar material is assumed to be homogeneous and linearly elastic, with constant Young's modulus E (force per unit area), as illustrated in Figure 1.

Figura 1 - Bar under normal force.

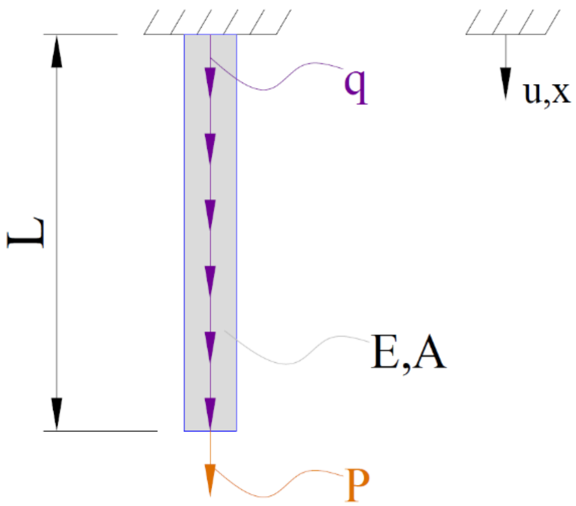

Source: own elaboration.

The objective of this Boundary Value Problem (BVP) is to determine the displacement, strain, and stress fields throughout the structural domain while satisfying the prescribed boundary conditions and applied loads. In the classical FEM, the displacement field u(x) is approximated directly, and the strain ε(x) and stress σ(x) fields are subsequently obtained through differentiation procedures.

In the HMSF, the displacement field $u_\Omega(x)$ and the stress field σ(x) within the domain Ω of each element (mixed formulation), as well as the independent displacement field $u_\Gamma(x)$ along the Γu portion of the static boundary (hybrid formulation), are simultaneously approximated. None of the fundamental relationships are satisfied a priori; instead, all governing field equations are established through the Weighted Residuals Method (WRM), ensuring that the discrete model consistently incorporates the essential properties of the continuum it represents.

The first step in defining the hybrid-mixed formulation consists of establishing the fundamental relationships governing the problem under analysis and identifying its main properties. In this context, let x represent the one-dimensional domain Ω, and let u(x), σ(x), and ε(x) denote the functions describing, respectively, the displacement, stress, and strain fields at all points of the bar domain ($0 \leq x \leq L$).

The governing equations associated with the problem illustrated in Figure 1, which characterize the proposed BVP, are presented below:

Equilibrium equation: The equilibrium of axial forces in an infinitesimal segment of length *dx* can be expressed by Eq. (1).

$$\frac{d\boldsymbol{\sigma}(\mathbf{x})}{dx} = \frac{-q}{A} \tag{1}$$

Compatibility equation: From the theory of elasticity, the compatibility relationship between the displacement field u(x) and the strain field ε(x) is obtained, as expressed in Eq. (2).

$$\boldsymbol{\varepsilon}(\mathbf{x}) = \mathbf{u}'(\mathbf{x}) = \frac{\partial \mathbf{u}}{\partial x} \tag{2}$$

Constitutive Law (Hooke's Law): The stress–strain relationship along the ***x***-direction is given by:

$$\boldsymbol{\sigma}(\mathbf{x}) = E\boldsymbol{\varepsilon}(\mathbf{x}) \tag{3}$$

Substituting Eq. (2.2) into Eq. (2.3) yields:

$$\boldsymbol{\sigma}(\mathbf{x}) = E\mathbf{u}'(\mathbf{x}) \tag{4}$$

From Eqs. (4) and (1), the following expression can be obtained:

$$\mathbf{u}''(\mathbf{x}) = -\frac{q}{EA} \tag{5}$$

Furthermore, for the bar subjected to axial loading, the stress field $\boldsymbol{\sigma}(\mathbf{x})$ is related to the axial force $\mathbf{N}(\mathbf{x})$ through the following expression:

$$\boldsymbol{\sigma}(\mathbf{x}) = \frac{\mathbf{N}(\mathbf{x})}{A} \tag{6}$$

Equation (5) represents the governing differential equation of the problem illustrated in Figure 1. For the complete definition of the strong-form BVP, it is also necessary to specify the corresponding boundary conditions.

Boundary conditions: Figure 1 shows that, at x = 0, the displacement is constrained to zero (Dirichlet or essential boundary condition), while at x = L the bar is subjected to an external axial force P acting on the boundary Γ_t (Neumann or natural boundary condition).

$$\mathbf{u}(0) = 0 \tag{7}$$

$$\mathbf{N}(L) = P \tag{8}$$

$$\boldsymbol{\sigma}(L) = \frac{\mathbf{N}(L)}{A} = \frac{P}{A} \tag{9}$$

By evaluating Eq. (4) at x=L, the following expression is obtained:

$$\boldsymbol{\sigma}(L) = E\mathbf{u}'(L) \tag{10}$$

Combining Eqs. (9) and (10) yields the boundary condition at x=L expressed in terms of the displacement field:

$$\mathbf{u}'(L) = \frac{P}{EA} \tag{11}$$

The BVP can now be formulated exclusively in terms of the displacement field u(x) through Eq. (5) and the boundary conditions given by Eqs. (7) and (11). Explicitly, the strong-form BVP associated with this problem is expressed as follows:

$$\mathbf{u}''(\mathbf{x}) + \frac{q}{EA} = 0 \qquad \text{in } 0 < \mathrm{x} < L \tag{12}$$

$$\mathbf{u}(0) = 0 \qquad \text{(Essential boundary condition - Dirichlet)} \tag{13}$$

$$\mathbf{u}'(\mathbf{L}) = \frac{P}{EA} \qquad \text{(Natural boundary condition – Neumann)} \tag{14}$$

The term **strong form** arises from the requirement that Eq. (12) must be satisfied at every point in the domain $0 < x < L$. In addition to satisfying the boundary conditions given by Eqs. (13) and (14), the displacement function u(x) must possess sufficient smoothness, being continuous together with its first and second derivatives, as required by Eq. (12). By integrating Eq. (12) twice and applying the corresponding boundary conditions, the analytical solution for the displacement field u(x) can be obtained, as shown in Eq. (15). The strain field ε(x) is then determined from the derivative of the displacement field according to Eq. (16), while the stress field σ(x) is obtained from Eq. (17). The equations presented below characterize the exact solution of the one-dimensional BVP in its strong form.

$$\mathbf{u}(\mathbf{x}) = \frac{-q}{EA}\frac{\mathbf{x}^2}{2} + \frac{(P+qL)\mathbf{x}}{EA} \tag{15}$$

$$\mathbf{u}'(\mathbf{x}) = \boldsymbol{\varepsilon}(\mathbf{x}) = \frac{-q\mathbf{x}}{EA} + \frac{(P+qL)}{EA} \quad (16)$$

$$\boldsymbol{\sigma}(\mathbf{x}) = E\boldsymbol{\varepsilon}(\mathbf{x}) = \frac{-q\mathbf{x}}{A} + \frac{(P+qL)}{A} \quad (17)$$

In the so-called **weak form**, the BVP is formulated in terms of an approximate solution $\tilde{\mathbf{u}}(\mathbf{x})$. With the introduction of $\tilde{\mathbf{u}}(\mathbf{x})$, Eq. (12) is no longer satisfied exactly at every point of the domain x, and a residual function R(x) is generated, as shown in Eq. (18).

$$\mathbf{u}''(\mathbf{x}) + \frac{q}{EA} = \mathbf{R}(\mathbf{x}) \qquad \text{in } 0 < x < L \qquad (18)$$

The objective is to minimize the residual function R(x) in a weighted-average sense. To accomplish this, the WRM is employed.

$$\int_0^L \mathbf{R}(\mathbf{x})\mathbf{w}(\mathbf{x})\mathbf{dx} \qquad (19)$$

where w(x) is a weighting function that must satisfy the homogeneous form of the essential (Dirichlet) boundary conditions associated with the BVP.

The development presented up to Eq. (17) describes the strong form of the bar problem subjected to axial loading and highlights the formulation of this problem from the perspective of Elasticity Theory, as well as its solution using the classical FEM through the application of Eq. (19).

In the following, to facilitate the reader's understanding of the application of the HMSF to the one-dimensional problem considered herein, it is necessary to derive an integral form of the complete set of governing equations. This approach differs from the classical FEM, in which the weighted integration procedure is applied exclusively to the residual equation represented by Eq. (18).

The HMSF involves the simultaneous approximation of three fields expressed in weighted integral form: the stress and displacement fields within the domain Ω, and the displacement field along the boundary Γ. To this end, Eq. (2.2) can be rewritten in the form of Eq. (20). By expressing Hooke's law in terms of the material flexibility $f = \frac{1}{E}$, Eq. (3)

can be rewritten as Eq. (21). Finally, by combining Eqs. (20) and (21), a new relationship is obtained, as shown in Eq. (22).

$$\boldsymbol{\varepsilon}(\mathbf{x}) - \mathbf{u}'(\mathbf{x}) = \mathbf{0} \tag{20}$$

$$\boldsymbol{\varepsilon}(\mathbf{x}) = f\boldsymbol{\sigma}(\boldsymbol{x}) \text{ with } f = \frac{1}{E} \tag{21}$$

$$f\boldsymbol{\sigma}(\boldsymbol{x}) - \boldsymbol{u}'(\boldsymbol{x}) = \mathbf{0} \tag{22}$$

From the equilibrium equation, Eq. (1), Eq. (23) can be written, where $\mathbf{b_x} = \frac{q}{A}$ is defined as the body force per unit volume acting in the x -direction. The Cauchy stress vector is expressed as $\bar{\mathbf{t}} = \mathbf{n}\boldsymbol{\sigma}$, where n is the unit normal vector and σ is the stress acting on an imaginary surface perpendicular to n.

For the one-dimensional bar subjected to axial loading, the boundary traction at x = L is represented by the Cauchy stress vector $\bar{\mathbf{t}} = \boldsymbol{\sigma}(L) = \frac{\boldsymbol{P}}{\boldsymbol{A}}$. In the present problem, the unit normal vector n is equal to 1 because it has the same direction as the x -axis and the applied force *P*, as shown in Eq. (24).

$$\frac{d\boldsymbol{\sigma}(\mathbf{x})}{dx} + \mathbf{b_x} = \mathbf{0} \tag{23}$$

$$\boldsymbol{\sigma}(L) - \bar{\boldsymbol{t}}(L) = \mathbf{0} \tag{24}$$

Equations (22), (23), and (24), expressed in a one-dimensional setting, involve the stress σ(x), strain ε(x), and displacement u(x) fields and serve as the basis for establishing the weighted integral relationships through the Galerkin Weighted Residuals Method (WRM). This weighting process is performed from an energy-consistent perspective, taking into account the physical compatibility requirements associated with each governing equation. In the present work, the approximations are restricted to the case of linear elastic behavior.

Integration over the domain Ω is carried out within the limits $0 < x < L$, whereas the boundary Γ_t is associated with the prescribed static (traction) boundary condition.

Since the essential (Dirichlet) boundary conditions are satisfied in strong form, all remaining boundary conditions may be imposed in weak form through the use of appropriate weighting functions. From an energy-based perspective, the weighting functions employed in the HMSF are δu(x), associated with the equilibrium equation; $\delta\boldsymbol{u}_{\boldsymbol{\Gamma}}$ (x), associated with the Neumann boundary condition; and δσ(x), associated with the compatibility equation.

$$\int_0^L \delta\mathbf{u}(\mathbf{x})\left[\frac{d\boldsymbol{\sigma}(\mathbf{x})}{dx}+\mathbf{b}_{\mathbf{x}}\right]=0 \tag{25}$$

$$\delta\boldsymbol{u}_{\boldsymbol{\Gamma}}(L)[\boldsymbol{\sigma}(L)-\bar{\mathbf{t}}]=0 \tag{26}$$

$$\int_0^L \delta\boldsymbol{\sigma}(\mathbf{x})[f\boldsymbol{\sigma}(\mathbf{x})-\mathbf{u}'(\mathbf{x})]=0 \tag{27}$$

By applying integration by parts to the second term of Eq. (27) and enforcing the essential boundary condition, Eq. (28) is obtained. This equation highlights the independent fields that justify the HMSF framework: the displacement field uuu and the stress field σ within the domain Ω (mixed formulation), together with the independent displacement field $\boldsymbol{u}_{\boldsymbol{\Gamma}}$ on the Γ_t portion of the boundary (hybrid formulation). Owing to this distinctive characteristic, both the domain and boundary fields must be considered in the finite element discretization process.

Likewise, Eqs. (25) and (26) can be reformulated as shown in Eqs. (29) and (30), respectively. Equation (30) corresponds to an integral evaluated at x=L, where the expression is integrated over the boundary.

$$\int_0^L \delta\boldsymbol{\sigma}(\mathbf{x})f\boldsymbol{\sigma}(\mathbf{x})dx+\int_0^L \frac{d\delta\boldsymbol{\sigma}(\mathbf{x})}{dx}\mathbf{u}(\mathbf{x})\,dx-\delta\boldsymbol{\sigma}(L)\mathbf{u}_{\boldsymbol{\Gamma}}(L)=0 \tag{28}$$

$$\int_0^L \delta\mathbf{u}(\mathbf{x})\left[\frac{d\boldsymbol{\sigma}(\mathbf{x})}{dx}\right]dx=-\int_0^L \delta\mathbf{u}(\mathbf{x})\mathbf{b}_{\mathbf{x}}dx \tag{29}$$

$$-\delta\mathbf{u}_{\boldsymbol{\Gamma}}(L)\boldsymbol{\sigma}(L)=-\delta\mathbf{u}_{\boldsymbol{\Gamma}}(L)\bar{\mathbf{t}} \tag{30}$$

From the perspective of the approximate analysis of this problem using the HMSF, the displacement approximations in the domain and on the boundary are defined independently and are weakly enforced to be compatible through the relation given in Eq. (28). Consequently, separate numerical approximations are introduced for the domain Ω(x) and the Γ_t (x=L). The three independent approximate fields are expressed in terms of nodal interpolations associated with the n nodes of the adopted mesh. Thus, the approximations for the stress field in the domain, $\tilde{\boldsymbol{\sigma}}(\mathbf{x})$, the displacement field in the domain, $\tilde{\mathbf{u}}(\mathbf{x})$, and the displacement field on the boundary, $\tilde{\mathbf{u}}_{\boldsymbol{\Gamma}}(\mathbf{x})$, are defined as follows:

$$\tilde{\boldsymbol{\sigma}}(\mathbf{x}) = \boldsymbol{\phi}_j(x)\boldsymbol{\sigma}_j(x_j) \ \text{ com } j = 1, \dots, n \tag{31}$$

$$\tilde{\mathbf{u}}(\mathbf{x}) = \boldsymbol{\phi}_j(x)\mathbf{u}_j(x_j) \quad \text{com } j = 1, \dots, n \tag{32}$$

$$\tilde{\mathbf{u}}_{\boldsymbol{\Gamma}\mathbf{t}}(\mathbf{x}) = \boldsymbol{\phi}_j(x)\mathbf{u}_{\boldsymbol{\Gamma}_j}(x_j) \ \text{ com } j = 1, \dots, n \tag{33}$$

where $\boldsymbol{\phi}_j$ denotes the approximation (shape) function associated with node j of the discretization adopted in the analysis.

Following the classical procedure employed in the FEM, Galerkin's method is applied by constructing the weighting functions δσ(x), δu(x) u(x)δu(x), and $\delta u_{\Gamma t}$ (x) using the same approximation basis $\boldsymbol{\phi}$ adopted for the corresponding field variables. Thus, the weighting functions are defined as follows:

$$\delta\tilde{\boldsymbol{\sigma}}(\mathbf{x}) = \boldsymbol{\phi}_i(x)\delta\boldsymbol{\sigma}_i(x_i) \quad \text{com } i = 1, \dots, n \tag{34}$$

$$\delta\tilde{\mathbf{u}}(\mathbf{x}) = \boldsymbol{\phi}_i(x)\delta\mathbf{u}_i(x_i) \ \text{ com } i = 1, \dots, n \tag{35}$$

$$\delta\tilde{\mathbf{u}}_{\boldsymbol{\Gamma}\mathbf{t}}(\mathbf{x}) = \boldsymbol{\phi}_i(x)\delta\mathbf{u}_{\boldsymbol{\Gamma}_i}(x_i) \quad \text{com } i = 1, \dots, n \tag{36}$$

$\boldsymbol{\sigma}_j(x_j)$ represents the vector of nodal stress variables, while $\mathbf{u}_j(x_j)$ and $\mathbf{u}_{\boldsymbol{\Gamma}_j}(x_j)$ denote, respectively, the nodal vectors of the degrees of freedom associated with the displacement field in the domain and the displacement field on the boundary for all n nodes of a given discretization of the problem under analysis.

By substituting the previously defined approximations into Eqs. (28), (29), and (30), the following expressions are obtained:

$$(\int_0^L \boldsymbol{\phi}_i(x) f \boldsymbol{\phi}_j(x) dx) \boldsymbol{\sigma}_j(x_j) + (\int_0^L \boldsymbol{\phi}'_i(x) \boldsymbol{\phi}_j(x) dx) \mathbf{u}_j(x_j) - (\boldsymbol{\phi}_i(L) \boldsymbol{\phi}_j(L)) u_{\Gamma_j}(x_j) = 0 \tag{37}$$

$$\left(\int_0^L \boldsymbol{\phi}'_i(x) \boldsymbol{\phi}_j(x) dx\right) \mathbf{u}_j(x_j) = -\int_0^L \boldsymbol{\phi}_i(x) \mathbf{b}_x dx \tag{38}$$

$$\left(-\boldsymbol{\phi}_i(L) \boldsymbol{\phi}_j(L)\right) \mathbf{u}_{\boldsymbol{\Gamma}_j}(x_j) = -\boldsymbol{\phi}_i(L) \bar{\mathbf{t}} \tag{39}$$

Using these three approximation fields, the linear system of equations associated with the HMSF can be obtained in the following form:

$$\begin{bmatrix} \mathbf{F}_{\boldsymbol{\Omega}} & \mathbf{A}_{\boldsymbol{\Omega}} & \mathbf{A}_{\boldsymbol{\Gamma}\mathbf{t}} \\ \mathbf{A}_{\boldsymbol{\Omega}}^{\mathrm{T}} & \mathbf{0} & \mathbf{0} \\ \mathbf{A}_{\boldsymbol{\Gamma}\mathbf{t}}^{\mathrm{T}} & \mathbf{0} & \mathbf{0} \end{bmatrix} \begin{Bmatrix} \mathbf{s}_{\boldsymbol{\Omega}} \\ \mathbf{q}_{\boldsymbol{\Omega}} \\ \mathbf{q}_{\boldsymbol{\Gamma}} \end{Bmatrix} = \begin{Bmatrix} \boldsymbol{e}_{\boldsymbol{\Gamma}_{\boldsymbol{u}}} \\ -\mathbf{Q}_{\boldsymbol{\Omega}} \\ -\mathbf{Q}_{\boldsymbol{\Gamma}_{\mathbf{t}}} \end{Bmatrix} \tag{40}$$

The vectors and matrices that define the HMSF system of equations are presented below:

$$\mathbf{F}_{\boldsymbol{\Omega}} = \mathbf{F}_{\boldsymbol{ij}} = \int_0^L \boldsymbol{\phi}_i(x) f \boldsymbol{\phi}_j(x) dx \tag{41}$$

$$\mathbf{A}_{\boldsymbol{\Omega}} = \mathbf{A}_{\boldsymbol{\Omega}_{ij}} = \int_0^L \boldsymbol{\phi}'_i(x) \boldsymbol{\phi}_j(x) dx \tag{42}$$

$$\mathbf{A}_{\boldsymbol{\Gamma}\mathbf{t}} = \mathbf{A}_{\boldsymbol{\Gamma}\mathbf{t}_{\mathbf{ij}}} = -(\boldsymbol{\phi}_i(L) \boldsymbol{\phi}_j(L)) \tag{43}$$

$$\mathbf{Q}_{\boldsymbol{\Omega}} = \mathbf{Q}_{\boldsymbol{\Omega}_{ij}} = \int_0^L \boldsymbol{\phi}_i(x) \mathbf{b}_x dx \tag{44}$$

$$\mathbf{Q}_{\Gamma_t} = \mathbf{Q}_{\Gamma_{t_i}} = \boldsymbol{\Phi}_i(L)\bar{\mathbf{t}} \tag{45}$$

$$\boldsymbol{e}_{\Gamma_u} = \mathbf{0}, \mathbf{s}_\Omega = \boldsymbol{\sigma}_j(x_j) \ , \mathbf{q}_\Omega = \mathbf{u}_j(x_j) \quad \text{e } \mathbf{q}_\Gamma = \mathbf{u}_{\Gamma_j}(x_j) \tag{46}$$

2.1.1 Solution of the HMSF Linear System of Equations Using the Babuška Method

The linear system arising from the HMSF, as represented by Eq. (40), is symmetric, sparse, and linearly dependent. Consequently, it cannot be solved directly using conventional solution procedures. This subsection presents a numerical technique originally introduced by Babuška and co-authors (STROUBOULIS; BABUŠKA; COPPS, 2000) and later adapted to the HMSF framework by Góis (2009) and Góis and Proença (2012), which enables the solution of this system.

The so-called Babuška method consists of modifying the original system in such a way that it becomes solvable while preserving the essential characteristics of the formulation. For the development of this procedure, the HMSF system is considered in the following form:

$$\boldsymbol{A}\mathbf{x} = \mathbf{b} \tag{47}$$

where:

$$\mathbf{A} = \begin{bmatrix} \mathbf{F}_\Omega & \mathbf{A}_\Omega & \mathbf{A}_{\Gamma t} \\ \mathbf{A}_\Omega^\mathbf{T} & \mathbf{0} & \mathbf{0} \\ \mathbf{A}_{\Gamma t}^\mathbf{T} & \mathbf{0} & \mathbf{0} \end{bmatrix}; \mathbf{x} = \begin{Bmatrix} \mathbf{s}_\Omega \\ \mathbf{q}_\Omega \\ \mathbf{q}_\Gamma \end{Bmatrix} \text{ e } \mathbf{b} = \begin{Bmatrix} \boldsymbol{e}_{\Gamma_u} \\ -\mathbf{Q}_\Omega \\ -\mathbf{Q}_{\Gamma_t} \end{Bmatrix} \tag{48}$$

The eigenvalues obtained from the coefficient matrix defined in Eq. (48), after the application of the boundary conditions, possess a clear physical interpretation. The positive eigenvalues are associated with the stress variables, whereas the negative eigenvalues correspond to the displacement variables in the domain together with the boundary displacement variables. The zero eigenvalues are related to spurious kinematic modes (GÓIS, 2009).

The Babuška method proposes the introduction of a diagonal matrix B to modify the linear system given in Eq. (48), such that the coefficient matrix A (the sparse matrix containing the system submatrices) becomes nonsingular. Once the modified system has been obtained, its solution can be computed using the Cholesky decomposition method.

$$\boldsymbol{B} = \frac{\mathbf{1}}{\sqrt{\boldsymbol{diag}(\mathbf{F}_{\boldsymbol{\Omega}})}} \tag{49}$$

$$\overline{\boldsymbol{A}}\overline{\mathbf{x}} = \overline{\mathbf{b}} \tag{50}$$

Thus, after applying the Babuška method, the modified linear system can be expressed as follows:

$$\overline{\mathbf{A}} = \begin{bmatrix} \mathbf{BF_\Omega B} & \mathbf{BA_\Omega} & \mathbf{BA_{\Gamma t}} \\ \mathbf{BA_\Omega^T} & \mathbf{0} & \mathbf{0} \\ \mathbf{BA_{\Gamma t}^T} & \mathbf{0} & \mathbf{0} \end{bmatrix}; \overline{\mathbf{x}} = \begin{Bmatrix} \mathbf{B^{-1}s_\Omega} \\ \mathbf{q_\Omega} \\ \mathbf{q_\Gamma} \end{Bmatrix} \text{ and } \overline{\mathbf{b}} \begin{Bmatrix} \boldsymbol{e}_{\boldsymbol{\Gamma}_{\boldsymbol{u}}} \\ -\mathbf{Q_\Omega} \\ -\mathbf{Q_{\Gamma_t}} \end{Bmatrix} \tag{51}$$

It is worth noting that:

$$\boldsymbol{diag}(\mathbf{BF_\Omega}\boldsymbol{B}) = \mathbf{I} \tag{52}$$

The resulting approximation is given by Eq. (53). Since the coefficient matrix A is perturbed along its main diagonal by a small positive parameter ε, the modified system no longer contains zero entries on the diagonal and becomes nonsingular. Consequently, the perturbed linear system can be solved efficiently using a numerical procedure such as the Cholesky decomposition method.

$$\tilde{\mathrm{A}} = \overline{\mathbf{A}} + \varepsilon\mathbf{I} \tag{53}$$

The Babuška method can be summarized as presented below. It consists of an iterative algorithm in which a_j denotes the error associated with iteration j, while $\mathbf{r}_j$ represents the residual at iteration j, as described by Góis (2009).

$$j = 0;\ \bar{x}_0 = 0;\ \bar{\mathbf{r}}_{\mathbf{0}} = \bar{\mathbf{b}};$$

2- Solve the linear system $\tilde{\mathrm{A}}\mathbf{a}_j = \bar{\mathbf{r}}_j$;

3- $\bar{\mathbf{x}}_{j+1} = \bar{\mathbf{x}}_j + \mathbf{a}_j;$

4- $\bar{\mathbf{r}}_{j+1} = \bar{\mathbf{r}}_j - \bar{\mathbf{A}}_j \mathbf{a}_j;$

5- $j = j + 1;$

6- If $\left(\frac{\bar{\mathbf{r}}_j^T \bar{\mathbf{r}}_j}{\mathbf{x}_j^T \bar{\mathbf{A}}\, \bar{\mathbf{x}}_j}\right) >$ tol, then go back to step 2.

The algorithm presented above can be applied to the solution of problems formulated using the HMSF, HMSF-GFEM, or HMSF-SGFEM approaches.

2.2 Stable Generalized Finite Element Method

This chapter presents the SGFEM nodal enrichment technique, which will subsequently be employed in conjunction with the HMSF. As previously defined, nodal enrichment can be understood as the expansion of the approximation basis functions without the need to introduce additional nodes into the finite element discretization of a given problem.

A brief introduction to both the GFEM and SGFEM is provided in the context of the one-dimensional problem previously described in Section 2.1 and illustrated in Figure 1. To this end, the governing equations, enrichment functions, bubble functions, and interpolation functions employed in the nodal enrichment process are presented. Furthermore, the differences in the accuracy of the displacement and stress solutions obtained using the GFEM and SGFEM for the bar problem subjected to axial loading are investigated. A comparison of the conditioning of the stiffness matrices generated by these methods is also performed, taking the classical FEM as the reference formulation.

Following the theoretical introduction to the SGFEM, the method is coupled with the HMSF and applied to the one-dimensional problem under consideration. The objective is to evaluate the potential of the HMSF-SGFEM formulation with respect to both the improvement of displacement-field approximations and the conditioning of the HMSF coefficient matrix.

2.2.1 Generalized Finite Element Method

The Finite Element Method (FEM) has been increasingly employed over the past decades due to its robustness and effectiveness in solving a wide range of engineering and scientific problems. Nevertheless, there are situations in which the classical FEM formulation is unable to accurately represent the physical behavior of a system. Examples include problems involving nearly incompressible elasticity, where the accuracy and reliability of stress predictions may be significantly compromised, and where even relatively refined meshes can lead to poor approximations. To overcome such limitations, several unconventional finite element formulations have been proposed, among which the Generalized Finite Element Method (GFEM), also known in certain contexts as the Extended Finite Element Method (XFEM), stands out.

The GFEM has been widely employed in recent years for the solution of problems involving complex geometries, heterogeneous microstructures, discontinuities, and stress concentrations. Its development was motivated by the need to improve the numerical solution of problems for which the classical FEM requires extensive mesh refinement and significant user intervention. In many cases, such requirements lead to computationally expensive and inefficient analyses. By incorporating enrichment functions into the approximation space, the GFEM is able to capture important features of the solution more accurately, often reducing the need for excessive mesh refinement.

The main characteristic of the GFEM is the expansion of the approximation space of the classical FEM through the enrichment of its shape functions. Like the classical FEM, the GFEM is based on the Partition of Unity (PU) concept, which constitutes one of its main advantages. As a result, only limited modifications to an existing FEM code are required to incorporate enrichment functions with compact support.

Another important advantage of the method is its ability to incorporate prior knowledge of the solution directly into the approximation space through appropriately chosen enrichment functions. Furthermore, the possibility of applying selective enrichments provides the GFEM with a high degree of generality and flexibility, making it suitable for the analysis of a wide variety of engineering and scientific problems.

The main difference between the classical FEM and the GFEM and SGFEM formulations lies in the definition of the approximation functions. In both GFEM and SGFEM, the shape functions ϕ_i are associated with subdomains (ω_i), commonly referred to as **clouds**. Each cloud is formed by the collection of finite elements that share a common node i, as illustrated in Figure 2.

Figure 2 - Example of a cloud in a one-dimensional discretization using two-node linear finite elements.

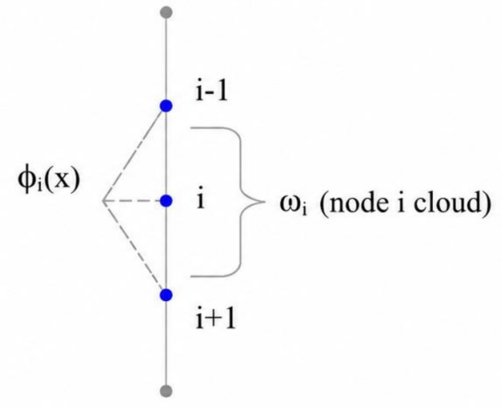

Source: own elaboration.

Within each cloud, the approximation functions associated with node iii are generated through the product of the enrichment functions ($\tilde{L}_i$), which may be polynomial or non-polynomial, and the Partition of Unity (PU) functions (ϕ_i) associated with the finite element mesh. Consequently, the main characteristics of the GFEM and SGFEM are the use of a cover mesh as the integration domain, the adoption of the conventional FEM Lagrangian shape functions as the Partition of Unity, and their enrichment through strategies derived from the Cloud Method (GÓIS, 2009).

The enriched shape functions employed in this work are identified by an asterisk (*) and can be defined as follows:

$$\phi_i^* = \phi_i \tilde{L}_i \tag{54}$$

Both monomials and polynomials may be employed as enrichment functions $\tilde{L}_i$, as shown in Eq. (55). The monomial bubble function (x-x_i) incorporates the coordinate of node i. The inclusion of this additional bubble function is necessary to preserve the physical interpretation of the original degrees of freedom and to ensure that the corresponding nodal displacement values remain unchanged. In the GFEM, enriched shape functions are constructed through the multiplication of the PU functions by these bubble functions, thereby introducing polynomial enrichment within the finite element.

$$\tilde{L}_i = \begin{cases} x \\ x^2 \end{cases} \text{ with } x = x - x_i \tag{55}$$

The purpose of the enrichment functions $\tilde{L}_i$ is to improve the quality of the local approximations. As previously mentioned, these functions may be defined based on prior knowledge of the expected solution. Figure 3 illustrates the construction of enriched functions in a two-dimensional domain.

However, the GFEM may present certain numerical difficulties because, in principle, virtually any function can be selected as an enrichment function. Consequently, the combination of the enrichment functions with the PU functions may lead to linear dependencies in the approximation space, resulting in stiffness matrices with condition numbers significantly larger than those obtained using the classical displacement-based FEM. This increase in the condition number may reduce the numerical accuracy of the computed solution.

A brief discussion of the condition number is presented later in this work. This parameter is commonly used to assess the conditioning of a linear system and can be applied to evaluate the stiffness matrices or coefficient matrices associated with the FEM, GFEM, SGFEM, HMSF, HMSF-GFEM, and HMSF-SGFEM formulations considered herein.

Figure 2 - Construction of a GFEM shape function using polynomial enrichment. Here, ϕ_i represents the Partition of Unity (PU) function, $\tilde{L}_i$ denotes the enrichment function, and ϕ_i^* corresponds to the enriched GFEM shape function.

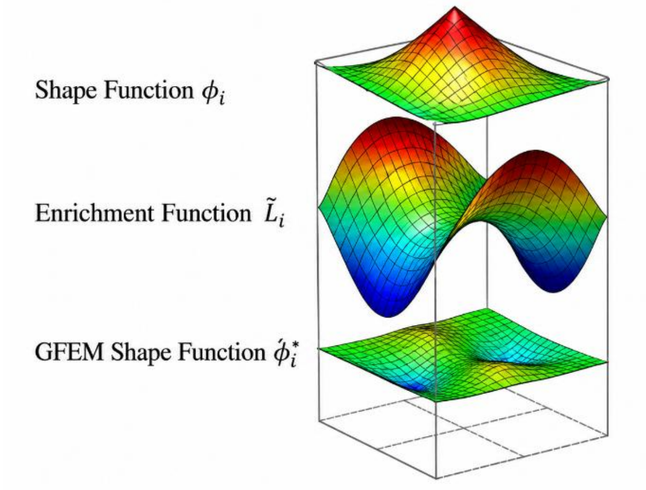

Source: adapted from Gupta et al. (2013).

In summary, the GFEM shares many characteristics with the classical FEM while providing greater flexibility for the analysis of complex engineering problems and facilitating its implementation in computational and commercial software environments. By enriching the approximation space, the GFEM is capable of producing highly accurate solutions with very low approximation errors, often using the same mesh employed in the classical FEM and at comparable computational costs (GUPTA et al., (2013)).

2.2.2 Stable Generalized Finite Element Method

The SGFEM is a variation of the GFEM whose primary objective is to preserve the favorable convergence properties of the approximation while improving the conditioning of the coefficient matrix of the resulting system. More specifically, the SGFEM seeks to achieve a level of matrix conditioning comparable to that of the classical FEM, since the stiffness matrix K generated by the GFEM may exhibit significantly poorer conditioning than that obtained with the conventional FEM (GUPTA et al., (2013)).

Another advantage of the SGFEM over the GFEM is its improved performance in regions where transitions occur between conventional and enriched elements. When selective enrichment is applied to a specific region of the mesh, three distinct categories of elements can be identified, as illustrated in Figure 4.

The first category consists of standard elements, in which none of the nodes are enriched. The second category comprises elements whose nodes share the same enrichment functions. The third category includes mixed elements, in which only some nodes are enriched or where different enrichment functions are assigned to different nodes.

Elements belonging to the second category, in which all nodes are enriched, possess the Partition of Unity property, whereby the sum of the PU functions is equal to one. As a consequence, the enrichment functions can be reproduced exactly within these elements. In contrast, mixed elements do not generally preserve this property. Depending on the selected enrichment functions, the enriched approximation may not be reproduced exactly within the element, which can adversely affect the quality of the local approximation and, consequently, the accuracy of the global solution and its convergence rate.

Figure 3 – Categories of finite elements in the transition region: standard elements, fully enriched elements, and mixed elements.

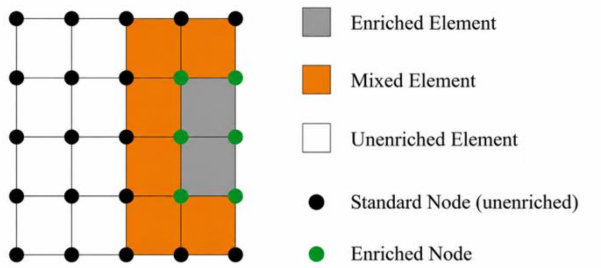

Source: own elaboration.

The SGFEM mitigates the effects associated with transition regions by modifying the enrichment functions in a manner that reduces their adverse influence on the convergence rate. As a result, the interaction between the different categories of elements illustrated in Figure 4 has a less pronounced impact on the quality of the approximation and on the overall convergence behavior of the method (GUPTA et al., (2013)).

Furthermore, the SGFEM is a highly robust method with respect to the choice of enrichment parameters. The fundamental difference between the SGFEM and the GFEM lies in the modification of the enrichment functions through the use of an interpolation operator. These modified enrichment functions are constructed so as to vanish at all nodes belonging to the cloud (ω_i) associated with the enrichment.

Accordingly, the SGFEM enrichment function is obtained within the cloud by taking the difference between the enrichment function $\tilde{L}_i$ and its interpolant I_{ω_i}. Thus, the modified enrichment function can be expressed as follows:

$$\tilde{L}_i^{SGFEM} = \tilde{L}_i - I_{\omega_i}(\tilde{L}_i) \qquad (56)$$

The interpolation function I_{ω_i} is defined as follows:

$$I_{\omega_i} = \sum_{j=1}^{N_e} \phi_j(x)\, \tilde{L}_i(x) \qquad (57)$$

Let $\mathbf{x}_j$ denote the coordinate of node j of the element under consideration, and let N_e represent the number of nodes in the element. Once the modified enrichment function has been constructed, the procedure for enriching the shape functions follows the same approach adopted in the GFEM and can be expressed as follows:

$$\phi_i^* = \phi_i \tilde{L}_i^{SGFEM} \qquad (58)$$

Figure 4 - Illustration of the SGFEM enrichment function obtained from the difference between the enrichment function and its interpolant.

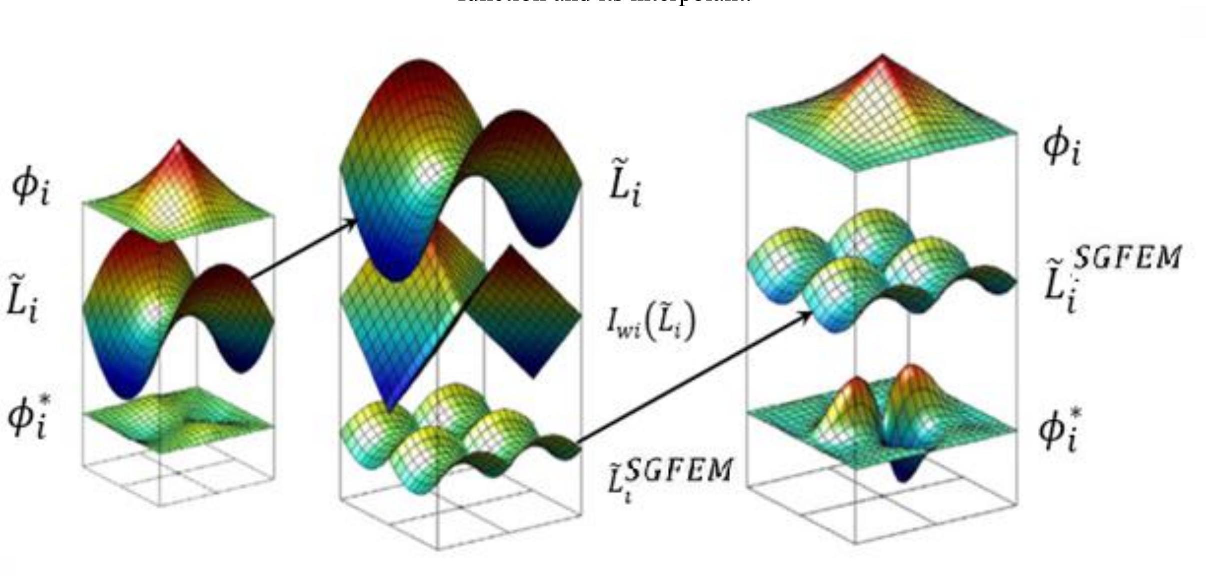

Source: adapted from Gupta et al. (2013).

In Figure 5, the illustration on the left depicts the construction of the enriched function used in the GFEM. The central illustration shows, from top to bottom, the original enrichment function $\tilde{L}_i$, the interpolation function I_{ω_i} , and the modified SGFEM enrichment function $\tilde{L}_i^{SGFEM}$. Finally, the illustration on the right presents the construction of the enriched SGFEM shape function ϕ_i^*.

NUMERICAL SIMULATIONS

3.1 EXAMPLE OF THE APPLICATION OF THE HMSF TO A ONE-DIMENSIONAL PROBLEM

The purpose of this subsection is to illustrate the application of the HMSF through a one-dimensional example. To this end, the domain of the model presented in Figure 1 is discretized into two linear finite elements with two nodes each (m=2), resulting in a total of three nodes (i=3), as shown in Figure 2. Each node is associated with a shape function $\phi_i(x)$. For the sake of simplicity, the length of the bar is taken L=2, and the parameters P, q, and A are assumed to be constant and equal to unity.

Figure 1 - Finite element discretization of the one-dimensional bar using m=2 two-node elements.

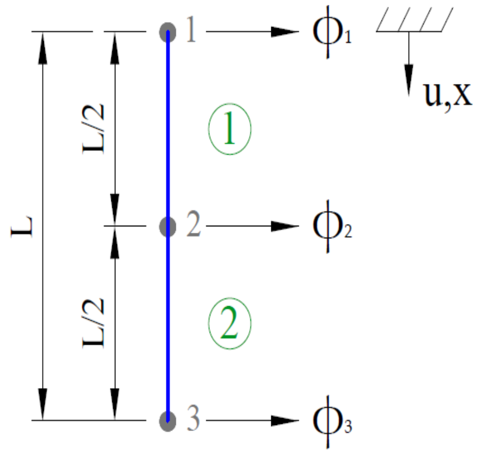

Source: own elaboration.

The definition of these shape functions follows the same methodology adopted in the finite element method through the **Partition of Unity (PU)** concept. According to this concept, the functions $\phi_i(x)$ must possess compact support; that is, they are nonzero only over a limited portion of the domain. Furthermore, when the shape function $\phi_i(x)$ is evaluated at the coordinate of its associated node i, it must assume the value of unity, $\phi_i(x_i)$=1, as illustrated in Figure 7.

Figure 2 - Partition of Unity (PU) shape functions for the one-dimensional bar problem.

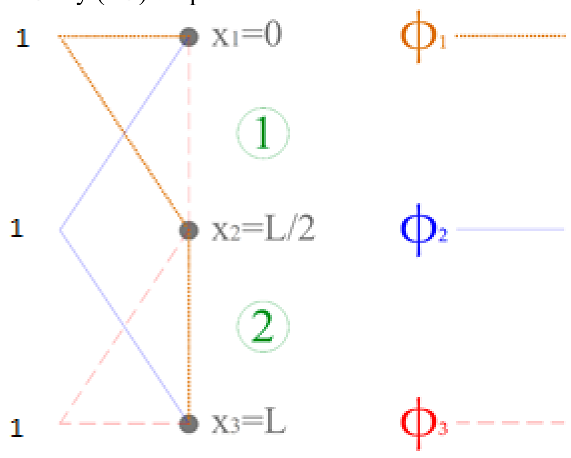

Source: own elaboration.

After discretizing the problem into three nodes and associating the linear shape functions $\phi_1(x)$, $\phi_2(x)$, and $\phi_3(x)$ with the corresponding subdomains of the two finite elements, as illustrated in Figure 7, the following expressions are obtained:

$$\phi_1(x) = \begin{cases} \dfrac{-2x}{L} + 1, & 0 \leq x \leq \dfrac{L}{2} \\ 0, & \dfrac{L}{2} \leq x \leq L \end{cases} \tag{59}$$

$$\phi_2(x) = \begin{cases} \dfrac{2x}{L}, & 0 \leq x \leq \dfrac{L}{2} \\ \dfrac{-2x}{L} + 2, & \dfrac{L}{2} \leq x \leq L \end{cases} \tag{60}$$

$$\phi_3(x) = \begin{cases} 0, & 0 \leq x \leq \dfrac{L}{2} \\ \dfrac{2x}{L} - 1, & \dfrac{L}{2} \leq x \leq L \end{cases} \tag{61}$$

By substituting the value L =2 into the previous set of equations, the shape functions and their corresponding derivatives over the two intervals can be expressed as follows:

$$\phi_1(x) = -x + 1$$

$$\phi_1'(x) = -1$$

$$\phi_2(x) = x \qquad 0 \leq x \leq \frac{L}{2} \tag{62}$$

$$\phi_2'(x) = 1$$

$$\phi_3(x) = 0$$

$$\phi_3'(x) = 0$$

$$\phi_1(x) = 0$$

$$\phi_1'(x) = 0 \tag{63}$$

$$\phi_2(x) = -x + 2 \qquad \frac{L}{2} \leq x \leq L$$

$$\phi_2'(x) = -1$$

$$\phi_3(x) = x - 1$$

$$\phi_3'(x) = 1$$

The detailed derivation of the HMSF submatrices for the example shown in Figure 2, based on the developments presented in Section 2.1, is available in the last author's GitHub repository (file **HMSF_1D_2_elements_L=2.sm**), as indicated in Section 5 of this work. Using the previously derived expressions for the case of m=2 elements and i=3 nodes, the resulting linear system of equations can be assembled and written in matrix form, as shown in Eq. (64).

$$\begin{bmatrix} F_{11} & F_{12} & F_{13} & \mathrm{A}_{\Omega_{11}} & \mathrm{A}_{\Omega_{12}} & \mathrm{A}_{\Omega_{13}} & \mathrm{A}_{\Gamma t_{11}} & \mathrm{A}_{\Gamma t_{12}} & \mathrm{A}_{\Gamma t_{13}} \\ F_{21} & F_{22} & F_{23} & \mathrm{A}_{\Omega_{21}} & \mathrm{A}_{\Omega_{22}} & \mathrm{A}_{\Omega_{23}} & \mathrm{A}_{\Gamma t_{21}} & \mathrm{A}_{\Gamma t_{22}} & \mathrm{A}_{\Gamma t_{23}} \\ F_{31} & F_{32} & F_{33} & \mathrm{A}_{\Omega_{31}} & \mathrm{A}_{\Omega_{32}} & \mathrm{A}_{\Omega_{33}} & \mathrm{A}_{\Gamma t_{31}} & \mathrm{A}_{\Gamma t_{32}} & \mathrm{A}_{\Gamma t_{33}} \\ \mathrm{A}_{\Omega_{11}} & \mathrm{A}_{\Omega_{21}} & \mathrm{A}_{\Omega_{31}} & 0 & 0 & 0 & 0 & 0 & 0 \\ \mathrm{A}_{\Omega_{12}} & \mathrm{A}_{\Omega_{22}} & \mathrm{A}_{\Omega_{32}} & 0 & 0 & 0 & 0 & 0 & 0 \\ \mathrm{A}_{\Omega_{13}} & \mathrm{A}_{\Omega_{23}} & \mathrm{A}_{\Omega_{33}} & 0 & 0 & 0 & 0 & 0 & 0 \\ \mathrm{A}_{\Gamma t_{11}} & \mathrm{A}_{\Gamma t_{21}} & \mathrm{A}_{\Gamma t_{31}} & 0 & 0 & 0 & 0 & 0 & 0 \\ \mathrm{A}_{\Gamma t_{12}} & \mathrm{A}_{\Gamma t_{22}} & \mathrm{A}_{\Gamma t_{32}} & 0 & 0 & 0 & 0 & 0 & 0 \\ \mathrm{A}_{\Gamma t_{13}} & \mathrm{A}_{\Gamma t_{23}} & \mathrm{A}_{\Gamma t_{33}} & 0 & 0 & 0 & 0 & 0 & 0 \end{bmatrix} *$$

$$\begin{pmatrix} \mathrm{s}_{\Omega_1} \\ \mathrm{s}_{\Omega_2} \\ \mathrm{s}_{\Omega_3} \\ \mathrm{q}_{\Omega_1} \\ \mathrm{q}_{\Omega_2} \\ \mathrm{q}_{\Omega_3} \\ \mathrm{q}_{\Gamma_1} \\ \mathrm{q}_{\Gamma_2} \\ \mathrm{q}_{\Gamma_3} \end{pmatrix} = \begin{pmatrix} e_{\Gamma_{u1}} \\ e_{\Gamma_{u2}} \\ e_{\Gamma_{u3}} \\ -\mathrm{Q}_{\Omega_1} \\ -\mathrm{Q}_{\Omega_2} \\ -\mathrm{Q}_{\Omega_3} \\ -\mathrm{Q}_{\Gamma_{t_1}} \\ -\mathrm{Q}_{\Gamma_{t_2}} \\ -\mathrm{Q}_{\Gamma_{t_3}} \end{pmatrix} \quad (64)$$

Substituting the previously computed values into the linear system, it can be observed that, unlike the submatrix **F**, which is associated exclusively with the stress field and is symmetric, the displacement-related submatrices $\mathbf{A_{\Omega}}$ and $\mathbf{A_{\Gamma t}}$ are generally nonsymmetric, as shown in Eqs. (65) and (66a).

The resulting linear system can be further reduced by enforcing the boundary conditions prescribed for the example. Specifically, at x=0, the boundary degree of freedom satisfies $\mathrm{q}_{\Gamma_1} = 0$. In addition, the eighth row and column of the coefficient matrix, as well as the eighth entry of the right-hand-side vector in Eq. (65), are eliminated. These terms are associated with boundary node 2 and do not contribute to $\mathbf{A_{\Gamma t}}$ (Eq. (43)) or to $\mathbf{Q_{\Gamma_t}}$ (Eq. (45)), owing to the particular characteristics of the HMSF formulation regarding domain nodes. The resulting reduced system is presented in Eq. (66).

$$\begin{bmatrix} F_{11} & F_{12} & F_{13} & \mathrm{A}_{\Omega_{11}} & \mathrm{A}_{\Omega_{12}} & \mathrm{A}_{\Omega_{13}} & \mathrm{A}_{\Gamma t_{13}} \\ F_{12} & F_{22} & F_{23} & \mathrm{A}_{\Omega_{21}} & \mathrm{A}_{\Omega_{22}} & \mathrm{A}_{\Omega_{23}} & \mathrm{A}_{\Gamma t_{23}} \\ F_{13} & F_{23} & F_{33} & \mathrm{A}_{\Omega_{31}} & \mathrm{A}_{\Omega_{32}} & \mathrm{A}_{\Omega_{33}} & \mathrm{A}_{\Gamma t_{33}} \\ \mathrm{A}_{\Omega_{11}} & \mathrm{A}_{\Omega_{21}} & \mathrm{A}_{\Omega_{31}} & 0 & 0 & 0 & 0 \\ \mathrm{A}_{\Omega_{12}} & \mathrm{A}_{\Omega_{22}} & \mathrm{A}_{\Omega_{32}} & 0 & 0 & 0 & 0 \\ \mathrm{A}_{\Omega_{13}} & \mathrm{A}_{\Omega_{23}} & \mathrm{A}_{\Omega_{33}} & 0 & 0 & 0 & 0 \\ \mathrm{A}_{\Gamma t_{13}} & \mathrm{A}_{\Gamma t_{23}} & \mathrm{A}_{\Gamma t_{33}} & 0 & 0 & 0 & 0 \end{bmatrix} * \begin{pmatrix} \mathrm{s}_{\Omega_1} \\ \mathrm{s}_{\Omega_2} \\ \mathrm{s}_{\Omega_3} \\ \mathrm{q}_{\Omega_1} \\ \mathrm{q}_{\Omega_2} \\ \mathrm{q}_{\Omega_3} \\ \mathrm{q}_{\Gamma_3} \end{pmatrix} = \begin{pmatrix} e_{\Gamma_{u1}} \\ e_{\Gamma_{u2}} \\ e_{\Gamma_{u3}} \\ -\mathrm{Q}_{\Omega_1} \\ -\mathrm{Q}_{\Omega_2} \\ -\mathrm{Q}_{\Omega_3} \\ -\mathrm{Q}_{\Gamma_{t3}} \end{pmatrix} \tag{65}$$

$$\begin{bmatrix} \frac{1}{3} & \frac{1}{6} & 0 & -\frac{1}{2} & -\frac{1}{2} & 0 & 0 & 0 & 0 \\ \frac{1}{6} & \frac{2}{3} & \frac{1}{6} & \frac{1}{2} & 0 & -\frac{1}{2} & 0 & 0 & 0 \\ 0 & \frac{1}{6} & 0 & 0 & \frac{1}{2} & \frac{1}{2} & 0 & 0 & -1 \\ -\frac{1}{2} & \frac{1}{2} & 0 & 0 & 0 & 0 & 0 & 0 & 0 \\ -\frac{1}{2} & 0 & \frac{1}{2} & 0 & 0 & 0 & 0 & 0 & 0 \\ 0 & -\frac{1}{2} & \frac{1}{2} & 0 & 0 & 0 & 0 & 0 & 0 \\ 0 & 0 & 0 & 0 & 0 & 0 & 1 & 0 & 0 \\ 0 & 0 & 0 & 0 & 0 & 0 & 0 & 0 & 0 \\ 0 & 0 & -1 & 0 & 0 & 0 & 0 & 0 & 0 \end{bmatrix} * \begin{pmatrix} \mathrm{s}_{\Omega_1} \\ \mathrm{s}_{\Omega_2} \\ \mathrm{s}_{\Omega_3} \\ \mathrm{q}_{\Omega_1} \\ \mathrm{q}_{\Omega_2} \\ \mathrm{q}_{\Omega_3} \\ \mathrm{q}_{\Gamma_1} \\ \mathrm{q}_{\Gamma_2} \\ \mathrm{q}_{\Gamma_3} \end{pmatrix} = \begin{pmatrix} 0 \\ 0 \\ 0 \\ \frac{1}{2} \\ 1 \\ \frac{1}{2} \\ 0 \\ 0 \\ 1 \end{pmatrix} \tag{66a}$$

$$\begin{bmatrix} \frac{1}{3} & \frac{1}{6} & 0 & -\frac{1}{2} & -\frac{1}{2} & 0 & 0 \\ \frac{1}{6} & \frac{2}{3} & \frac{1}{6} & \frac{1}{2} & 0 & -\frac{1}{2} & 0 \\ 0 & \frac{1}{6} & 0 & 0 & \frac{1}{2} & \frac{1}{2} & -1 \\ -\frac{1}{2} & -\frac{1}{2} & 0 & 0 & 0 & 0 & 0 \\ -\frac{1}{2} & 0 & \frac{1}{2} & 0 & 0 & 0 & 0 \\ 0 & -\frac{1}{2} & \frac{1}{2} & 0 & 0 & 0 & 0 \\ 0 & 0 & -1 & 0 & 0 & 0 & 0 \end{bmatrix} * \begin{pmatrix} \mathrm{s}_{\Omega_1} \\ \mathrm{s}_{\Omega_2} \\ \mathrm{s}_{\Omega_3} \\ \mathrm{q}_{\Omega_1} \\ \mathrm{q}_{\Omega_2} \\ \mathrm{q}_{\Omega_3} \\ \mathrm{q}_{\Gamma_3} \end{pmatrix} = \begin{pmatrix} 0 \\ 0 \\ 0 \\ \frac{1}{2} \\ 1 \\ \frac{1}{2} \\ 1 \end{pmatrix} \tag{66b}$$

The linear system represented by Eq. (66b) can be solved using the Babuška method presented previously in Section 2.2. For this purpose, a MatLab® program was developed and employed in the numerical solution of the problem. The corresponding source code is available in the last author's GitHub repository (files **HMSF_1D_2_elements.m** and **cholesky.m**).

By applying the computational implementation described above, the following results are obtained:

$$\begin{pmatrix} s_{\Omega_1} \\ s_{\Omega_2} \\ s_{\Omega_3} \\ q_{\Omega_1} \\ q_{\Omega_2} \\ q_{\Omega_3} \\ q_{\Gamma_1} \\ q_{\Gamma_2} \\ q_{\Gamma_3} \end{pmatrix} = \begin{pmatrix} 3 \\ 2 \\ 1 \\ -0{,}444 \\ 3{,}111 \\ 3{,}5556 \\ 0 \\ 0 \\ 4 \end{pmatrix} \tag{67}$$

The results reported in Eq. (67) are evaluated through comparisons between the exact and numerical solutions obtained using the HMSF. Both the displacement and stress distributions over the domain are analyzed, as shown in Figures 4 and 5.

The exact displacement and strain solutions for the model problem can be obtained by substituting the values L=2 and P=q=A=E=1 into Eqs. (15) and (16), respectively. This yields the following expressions:

$$\mathbf{u}(\mathrm{x}) = -\frac{\mathrm{x}^2}{2} + 3\mathrm{x} \tag{68}$$

$$\boldsymbol{\varepsilon}(\mathrm{x}) = -\mathrm{x} + 3 \tag{69}$$

Figure 3 - Comparison of the displacement field along the domain obtained from the exact solution, FEM, and HMSF using one-dimensional two-node elements.

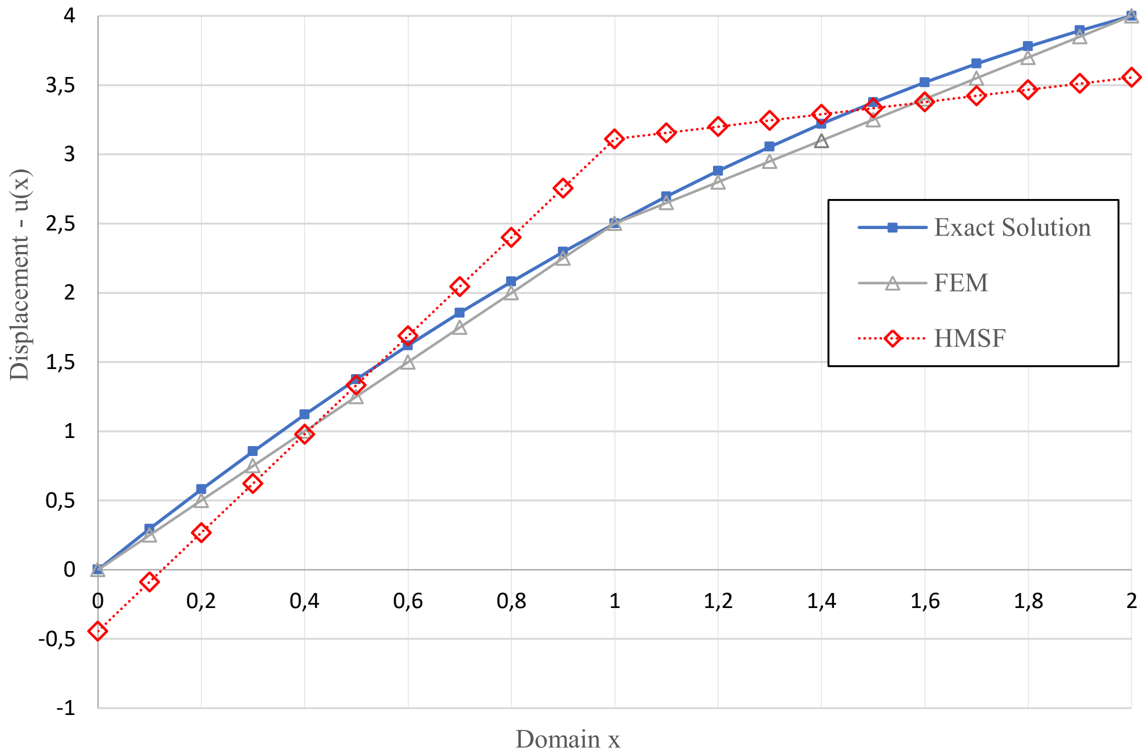

Source: own elaboration.

Figure 9 - Comparison of the stress distribution along the domain obtained from the exact solution, FEM, and HMSF using one-dimensional two-node elements.

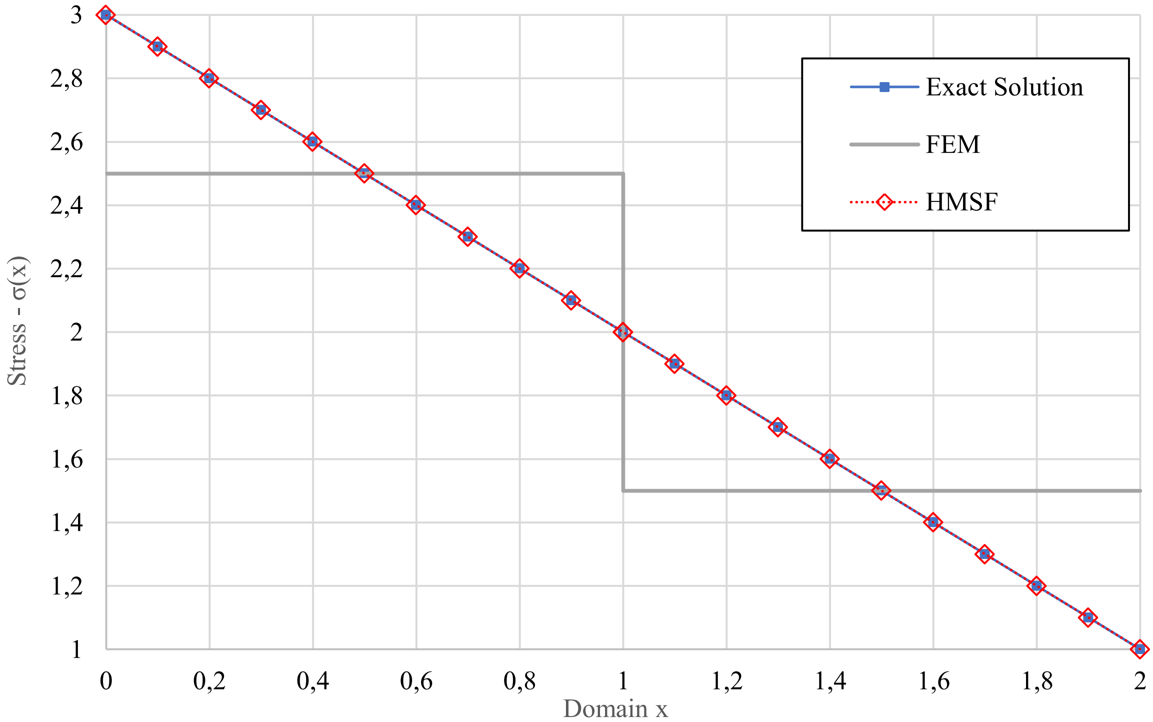

Source: own elaboration.

The performance of the HMSF is particularly noteworthy in the analysis of the stress field, for which the exact solution of the proposed problem is recovered. However, with respect to the displacement field, the approximation obtained using the HMSF is less accurate than that provided by the classical FEM.

To quantify the accuracy of the displacement approximation, the normalized L_2-error, denoted by $\bar{e}_{L_2}$, is employed and defined by Eq. (70). The accuracy of the stress field is evaluated using the error measure given by Eq. (71), denoted by $\bar{e}_{energy}$, which is also referred to as the **energy error**. The error values obtained for each formulation are summarized in Table 1.

$$\bar{e}_{L_2} = \frac{\|\mathbf{u}_{ex}(\mathrm{x}) - \mathbf{u}_h\|_{L_2}}{\|\mathbf{u}_{ex}(\mathrm{x})\|_{L_2}} = \frac{(\int_0^L (\mathbf{u}_{ex}(\mathrm{x}) - \mathbf{u}_h)^2\, d\mathrm{x})^{\frac{1}{2}}}{(\int_0^L (\mathbf{u}_{ex}(\mathrm{x}))^2\, d\mathrm{x})^{\frac{1}{2}}} \tag{70}$$

$$\bar{e}_{energy} = \frac{(\frac{1}{2}\int_0^L (\boldsymbol{\sigma}_{ex}(\mathrm{x}) - \boldsymbol{\sigma}_h)^2\, d\mathrm{x})^{\frac{1}{2}}}{(\frac{1}{2}\int_0^L (\boldsymbol{\sigma}_{ex}(\mathrm{x}))^2\, d\mathrm{x})^{\frac{1}{2}}} \tag{71}$$

where $\mathbf{u}_{ex}$ denotes the exact displacement solution and $\mathbf{u}_h$ represents the approximate displacement solution obtained using either the FEM or the HMSF. Similarly, $\boldsymbol{\sigma}_{ex}(\mathrm{x})$ denotes the exact stress field, while $\boldsymbol{\sigma}_h$ represents the corresponding approximate stress field computed by the numerical method under consideration.

Table 1 - Comparison of the normalized L_2-error and energy error obtained with the different numerical formulations.

Method	Error in displacement $\bar{e}_{L_2}$	Energy error $\bar{e}_{energy}$
FEM	3,50%	13,87%
HMSF	11,77%	0,00%

Source: own elaboration.

The results presented in Table 1 and Figures 8 and 9 highlight the potential of the HMSF for the representation of stress fields when compared with the classical FEM. For the problem considered, the HMSF is able to recover the exact stress solution, resulting in a zero stress error. In contrast, the displacement approximation obtained with the HMSF is less accurate than that provided by the classical FEM, leading to a larger displacement error.

3.2 APPLICATION OF THE GFEM TO A ONE-DIMENSIONAL (1D) PROBLEM

In Eq. (72), $\tilde{\mathbf{u}}$ denotes the enriched displacement vector associated with the augmented shape functions resulting from the application of the GFEM to the bar problem subjected to axial loading, considering *m=2* elements and *n=2* nodes per element. The functions ϕ_i^* represent the enriched shape functions associated with node i.

$$\tilde{\mathbf{u}} = \begin{pmatrix} \phi_1 & \phi_2 & \phi_{\mathbf{2}}^* & \phi_3 & \phi_{\mathbf{3}}^* \end{pmatrix} \begin{pmatrix} u_1 \\ u_2 \\ u_2^* \\ u_3 \\ u_3^* \end{pmatrix} \tag{72}$$

For the example illustrated in Figure 2, only two nodes are eligible for enrichment, since nodes subjected to essential (Dirichlet) boundary conditions are not enriched. The resulting enrichment scheme is shown in Figure 10.

Figure 4 - One-dimensional bar discretization showing the GFEM enrichment scheme, with nodes 2 and 3 selected for enrichment.

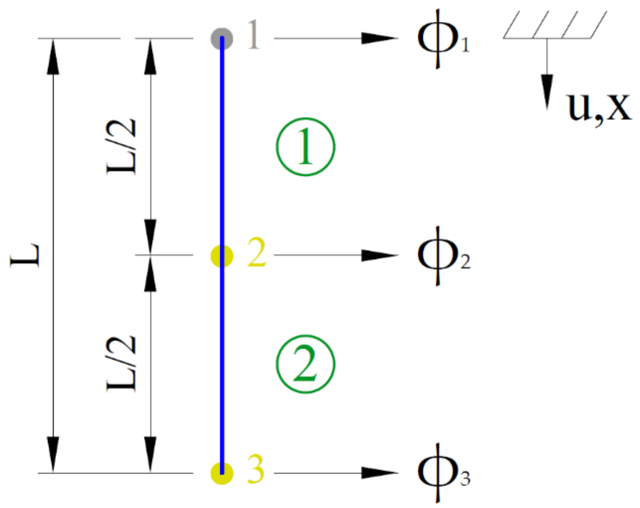

Source: own elaboration.

The enrichment function $\tilde{L}_i$ adopted in this example is a second-order polynomial and is defined as follows:

$$x = (x - x_i)^2 \tag{73}$$

Finally, in order to assemble the global linear system associated with the one-dimensional problem using the GFEM approximation, both the stiffness matrix and the force vector must be expanded to account for the additional degrees of freedom introduced by the enrichment functions. The computation of the enriched displacement vector $\tilde{\mathbf{u}}$ is then obtained from the resulting system of equations, as shown in Eq. (74).

$$\begin{bmatrix} k_{11} & k_{12} & k_{12^*} & k_{13} & k_{13^*} \\ k_{21} & k_{22} & k_{22^*} & k_{23} & k_{23^*} \\ k_{2^*1} & k_{2^*2} & k_{2^*2^*} & k_{2^*3} & k_{2^*3^*} \\ k_{31} & k_{32} & k_{32^*} & k_{33} & k_{33^*} \\ k_{3^*1} & k_{3^*2} & k_{3^*2^*} & k_{3^*3} & k_{3^*3^*} \end{bmatrix} \begin{pmatrix} u_1 \\ u_2 \\ u_2^* \\ u_3 \\ u_3^* \end{pmatrix} = \begin{pmatrix} f_1 \\ f_2 \\ f_2^* \\ f_3 \\ f_3^* \end{pmatrix} \tag{74}$$

The results obtained from the GFEM-enriched approximations applied to the one-dimensional problem illustrated in Figure 8 are presented and compared with the corresponding SGFEM solutions in the following section. In addition, a comparison of the condition numbers associated with the coefficient matrices arising from the FEM, GFEM, and SGFEM formulations is provided.

The condition number obtained from the classical FEM is adopted as a reference value, allowing a direct assessment of the effects of the enrichment strategies on the numerical conditioning of the resulting systems. This comparison provides insight into the numerical performance of the unconventional formulations investigated in this work.

3.3 APPLICATION OF THE SGFEM TO A ONE-DIMENSIONAL BAR SUBJECTED TO AXIAL LOADING

As in the previous section, this subsection presents the application of the SGFEM to the example illustrated in Figure 2. For the sake of consistency and comparison, the enrichment is applied to the same nodes considered in the GFEM analysis, namely those indicated in Figure 10.

For the one-dimensional problem under consideration, the enrichment function based on the quadratic term x^2 is defined as follows:

$$\tilde{L}_i^{SGFEM} = (x - x_i)^2 - \sum_{j=1}^{2} \phi_j(x)\,(x_j - x_i)^2 \tag{75}$$

As in the GFEM formulation, the assembly of the global linear system for the one-dimensional problem using the SGFEM approximation requires the expansion of both the coefficient matrix and the force vector in order to accommodate the additional degrees of freedom introduced by the enrichment functions.

$$\begin{bmatrix} k_{11} & k_{12} & k_{12^*} & k_{13} & k_{13^*} \\ k_{21} & k_{22} & k_{22^*} & k_{23} & k_{23^*} \\ k_{2^*1} & k_{2^*2} & k_{2^*2^*} & k_{2^*3} & k_{2^*3^*} \\ k_{31} & k_{32} & k_{32^*} & k_{33} & k_{33^*} \\ k_{3^*1} & k_{3^*2} & k_{3^*2^*} & k_{3^*3} & k_{3^*3^*} \end{bmatrix} \begin{pmatrix} u_1 \\ u_2 \\ u_2^* \\ u_3 \\ u_3^* \end{pmatrix} = \begin{pmatrix} f_1 \\ f_2 \\ f_2^* \\ f_3 \\ f_3^* \end{pmatrix} \tag{76}$$

3.3.1 Results of the Application of GFEM and SGFEM to the One-Dimensional Example

The results obtained in this chapter are evaluated through comparisons between the exact solution and the numerical solutions provided by the FEM, GFEM, and SGFEM formulations for both the displacement and stress fields throughout the domain, as illustrated in Figures 11 and 12. The detailed development of the equations associated with the problem under consideration is available in the last author's GitHub repository (file **FEM_GFEM_SGFEM_1D_2_elements_L=2**).

To provide a more quantitative assessment of the accuracy of the numerical formulations, the normalized L_2-error, $\bar{e}_{L_2}$, defined by Eq. (70), is employed to evaluate the displacement field. Similarly, the energy error, $\bar{e}_{energy}$, defined by Eq. (71), is used to assess the accuracy of the stress field. The corresponding results for the methods considered are summarized in Table 2.

Figure 5 - Comparison of displacement distributions along the domain obtained from the exact solution and from the HMSF, FEM, GFEM, and SGFEM formulations.

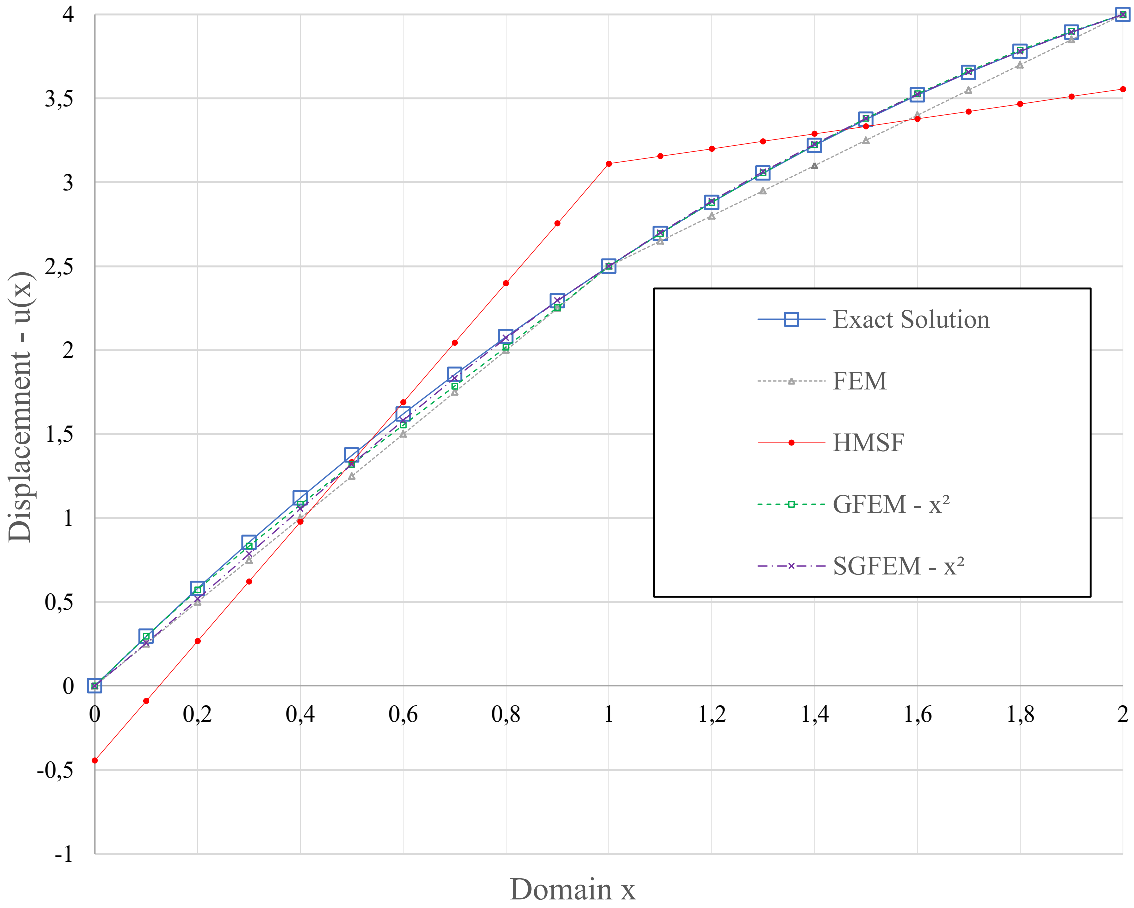

Source: own elaboration.

Figure 6 - Comparison of the stress field in the HMSF domain with the exact solution and the corresponding results obtained using the FEM, GFEM, and SGFEM formulations.

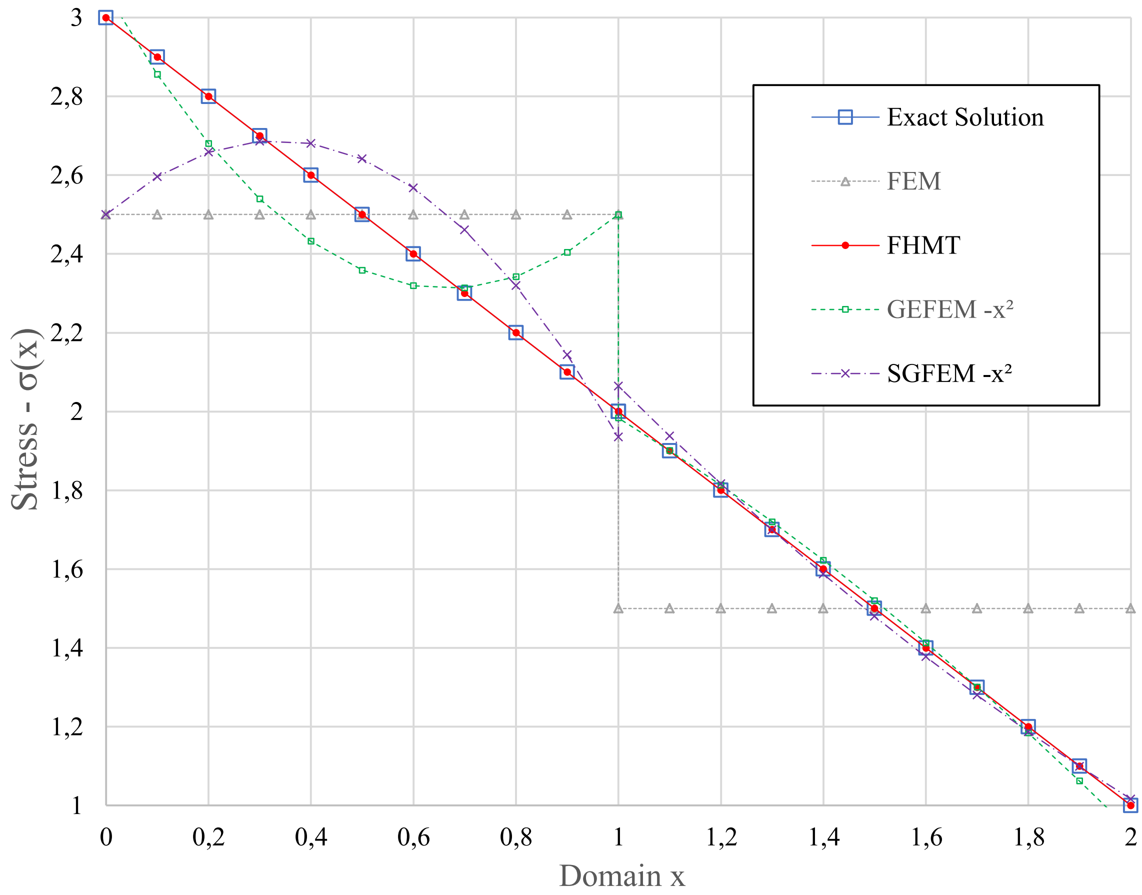

Source: own elaboration.

Table 1 Comparison of the normalized L_2-error and energy error obtained with the enrichment methods.

Method	Error in displacement $\bar{e}_{L_2}$	Energy error $\bar{e}_{energy}$
FEM	3,50%	13,87%
HMSF	11,77%	0,00%
GFEM	1,21%	6,10%
SGFEM	1,21%	6,10%

Source: own elaboration.

As shown in Table 2, the enrichment applied to the problem under consideration, whether through the GFEM or the SGFEM, locally increases the polynomial order of the approximation functions. This enhancement improves the accuracy of the displacement field and, consequently, the stress field, since the latter is obtained from the derivative of the displacement approximation.

It can also be observed that the HMSF provides a significantly more accurate recovery of the stress field when compared with the other formulations considered. Therefore, the main motivation for combining enrichment techniques with the HMSF is to improve the quality of the displacement approximations while preserving the excellent stress-field representation that characterizes the HMSF formulation.

3.4 CONDITIONING ANALYSIS OF THE LINEAR SYSTEMS ASSOCIATED WITH THE APPROXIMATE SOLUTIONS

In general, the conditioning of a linear system is closely related to the reliability and numerical stability of its solution. As an illustrative example, consider the linear system presented below, which may be associated with the FEM, GFEM, or SGFEM formulations.

$$[\mathbf{A}]\{\mathbf{x}\} = \{\mathbf{B}\} \tag{77}$$

where $[\mathbf{A}]$ is a sparse, symmetric, positive-definite coefficient matrix of order n x n. Let $\{\mathbf{x}\}$ denote the solution vector of the linear system, computed using a numerical solution procedure, such as a direct elimination method implemented in a linear algebra package. Formally, the solution can be expressed in terms of the inverse of the coefficient matrix as follows:

$$\{\mathbf{x}\} = [\mathbf{A}]^{-1}\{\mathbf{B}\} \tag{78}$$

The inverse matrix possesses several useful properties beyond providing a formal expression for the solution of the system. In particular, each of its entries can be interpreted as representing the response of a given degree of freedom to a unit excitation applied at another degree of freedom of the system.

A linear system of the form $[\mathbf{A}]\{\mathbf{x}\}=\{\mathbf{B}\}$ is said to be **well-conditioned** if small perturbations in the coefficient matrix $[\mathbf{A}]$ or in the right-hand-side vector $\{\mathbf{B}\}$ produce only small changes in the solution vector $\{\mathbf{x}\}$. Conversely, the system is considered **ill-conditioned** when small variations in $[\mathbf{A}]$ or $\{\mathbf{B}\}$ lead to disproportionately large changes in the computed solution. In such cases, numerical errors arising from round-off operations, discretization procedures, or uncertainties in the input data may be significantly amplified, thereby compromising the accuracy and reliability of the results.

The **condition number** is a scalar measure used to assess the sensitivity of the solution of a linear system to perturbations in the coefficient matrix and the right-hand-side vector. In practical terms, it provides an indication of the potential loss of numerical accuracy during the solution process.

A small condition number indicates that the system is **well-conditioned**, meaning that the computed solution is relatively insensitive to small perturbations and numerical errors. Conversely, a large condition number indicates that the system is **poorly conditioned**, so that even small perturbations may lead to significant changes in the solution. Such behavior is often associated with near-linear dependencies among the system equations or, equivalently, among the rows or columns of the coefficient matrix.

In the GFEM, since enrichment functions can be selected with considerable flexibility, the conditioning of the coefficient matrix [$\mathbf{A}$] may be significantly affected by both the mesh discretization and the enrichment strategy adopted. In particular, conditioning problems may arise when the enrichment functions exhibit characteristics similar to those of the Partition of Unity (PU) functions.

The examples presented in Sections 2.2.1 and 2.2.2 illustrate this situation. In those cases, both the PU functions and the enrichment functions are polynomial in nature, which may introduce near-linear dependencies into the approximation space. As a consequence, the resulting coefficient matrix can become ill-conditioned, leading to an increase in the condition number and a potential loss of numerical accuracy in the computed solution.

The condition number of the coefficient matrix [$\mathbf{A}$] is defined by:

$$\mathrm{Cond}[\mathbf{A}] = \|\mathbf{A}\|\left\|\mathbf{A}^{-1}\right\| \tag{79}$$

where,

$$\|\mathbf{A}\| = \sqrt{\sum_{i=1}^{n}\sum_{j=1}^{n} a_{ij}^2} \tag{80}$$

where a_{ij} denotes the (i,j)-th entry of the coefficient matrix [$\mathbf{A}$] .

3.5 APPLICATION OF THE HMSF-SGFEM TO A ONE-DIMENSIONAL PROBLEM

This chapter presents the formulation of the enriched HMSF-SGFEM elements for a one-dimensional example and provides a comparison among the FEM, HMSF, and HMSF-SGFEM approaches. The comparison is carried out with respect to both the approximation fields and the conditioning of the stiffness and coefficient matrices associated with the HMSF and HMSF-SGFEM formulations.

For the model represented in Figure 2, nodes 2 and 3 were selected for enrichment in the domain, affecting both the stress and displacement fields. Consequently, the boundary matrix $\mathbf{A}_{\mathbf{\Gamma t}}$ must also be expanded to ensure compatibility with the matrix operations required by the formulation, particularly the multiplication involving matrix **B**.

It is important to emphasize that, in order to guarantee the stability and solvability of the discrete HMSF linear systems, the **Inspection Test** originally proposed by Zienkiewicz (1986) and subsequently adapted to the HMSF by Góis (2009) must be satisfied. This test establishes the algebraic conditions required for the existence of a numerical solution to the HMSF system represented by Eq. (40), which can be expressed as follows:

$$\mathbf{s}_{\mathbf{\Omega}} \geq \mathbf{q}_{\mathbf{\Omega}} \tag{81}$$

$$\mathbf{s}_{\mathbf{\Omega}} \geq \mathbf{q}_{\mathbf{\Gamma}} \tag{82}$$

For the HMSF-GFEM and HMSF-SGFEM formulations, the **Inspection Test** must be extended to account for the additional degrees of freedom introduced by the enrichment procedure. In this case, new parameters associated with the stress field in the domain, represented by $\mathbf{b}_{ij}$, the displacement field in the domain, represented by $\mathbf{c}_{ij}$, and the displacement field on the boundary, represented by $\mathbf{d}_{ij}$, are incorporated into the test.

Accordingly, Eqs. (81) and (82) are modified and can be rewritten as follows:

$$\mathbf{s}_{\mathbf{\Omega}} + \mathbf{b}_{ij} \geq \mathbf{q}_{\mathbf{\Omega}} + \mathbf{c}_{ij} \tag{83}$$

$$\mathbf{s}_{\Omega} + \mathbf{b}_{ij} \geq \mathbf{q}_{\Gamma} + \mathbf{d}_{ij} \tag{84}$$

It is important to emphasize that the **Inspection Test** constitutes a **necessary, but not sufficient, condition** for guaranteeing the solvability of the system. Although satisfying this test is essential for the formulation to be admissible, it does not by itself ensure the existence of a unique numerical solution.

For the enriched system represented by Eq. (85), a sufficient condition for solvability can be established through an analysis of the physical interpretation of the eigenvalues of the coefficient matrix. As discussed by Góis (2009), the eigenvalue spectrum provides valuable information regarding the stability, admissibility, and solvability of the enriched HMSF formulation.

Despite the condition discussed above, for the one-dimensional problem considered it was possible to enrich the nodes associated with both the stress and displacement fields in the domain. Consequently, two enrichment strategies can be incorporated into the HMSF formulation.

For the sake of brevity, this section presents the formulation and application of the method only for the case of **SGFEM enrichment**, since the enrichment procedure based on the **GFEM** follows the same steps and differs only in the definition of the enrichment functions employed.

The implementation of enrichment in both domain fields—namely, the stress and displacement fields—within the matrix form of the HMSF linear system given by Eq. (65) is available in the last author's GitHub repository. The complete formulation and corresponding calculations can be found in the file **HMSF-SGFEM_1D_2_elements_L=2**.

The enrichment function adopted in this case is the same as that employed in Section 3.3 and defined by Eq. (75). By substituting the corresponding values obtained for the problem under consideration, a new linear system is obtained, incorporating the enriched shape functions associated with nodes 2 and 3.

However, this enriched system cannot be solved using a direct solution procedure. Even after applying the boundary conditions and reducing the system, the coefficient matrix AAA still contains zero entries on its main diagonal and, therefore, cannot be regarded as positive definite. Consequently, the **Cholesky decomposition** cannot be applied directly.

To overcome this difficulty, the **Babuška method**, described previously, is employed. In this approach, the coefficient matrix is suitably modified to produce a solvable system, after which the Cholesky decomposition can be used efficiently. The numerical solution of the resulting system was obtained using a MATLAB® implementation developed by the last author. The corresponding source code is available in the author's GitHub repository (files **HMSF_1D_2_elements.m** and **cholesky.m**).

The results can be evaluated through comparisons between the exact solution, the HMSF solution, and the solutions obtained using the **Hybrid-Mixed Stress Formulation enriched with the Generalized Finite Element Method (HMSF-GFEM)** and the **Stable Generalized Finite Element Method (HMSF-SGFEM)**. The comparison is carried out for both the displacement and stress fields throughout the domain, as illustrated in Figures 13 and 14.

Figure 7 - Comparison of the domain displacement obtained from the exact solution, FEM, HMSF, and the enriched formulations HMSF-GFEM and HMSF-SGFEM.

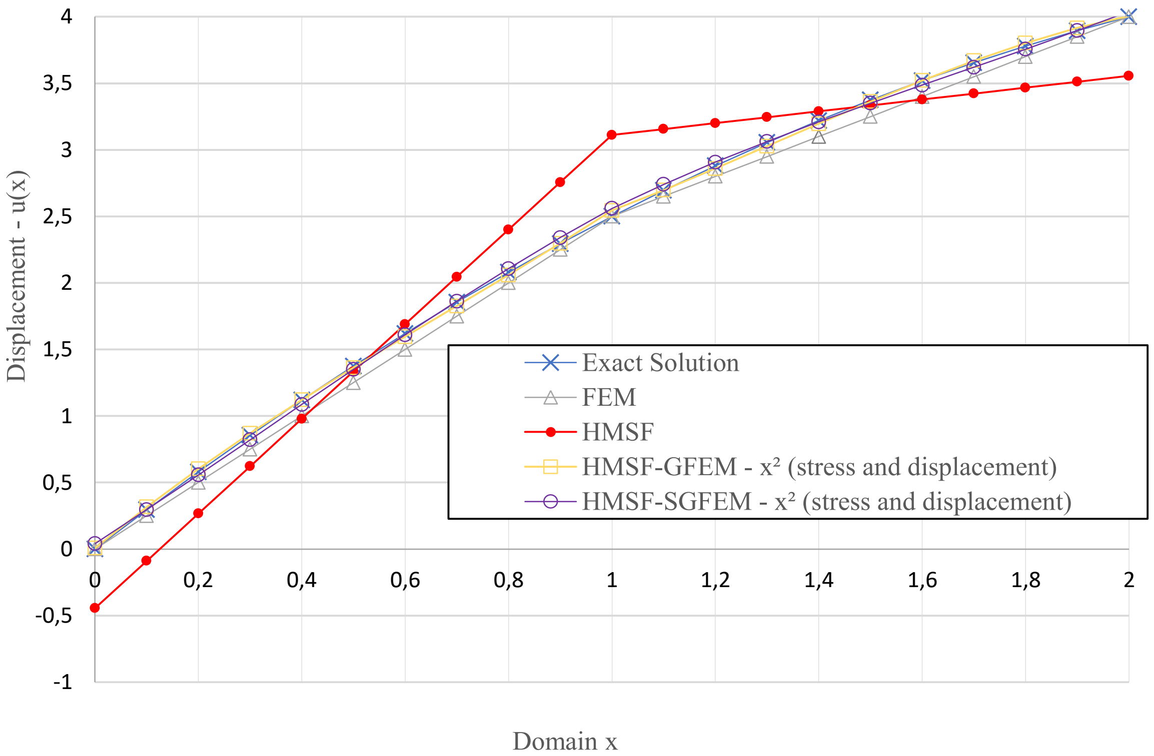

Source: own elaboration.

Figure 8 - Comparison of the stress obtained from the exact solution, FEM, HMSF, and the enriched formulations HMSF-GFEM and HMSF-SGFEM.

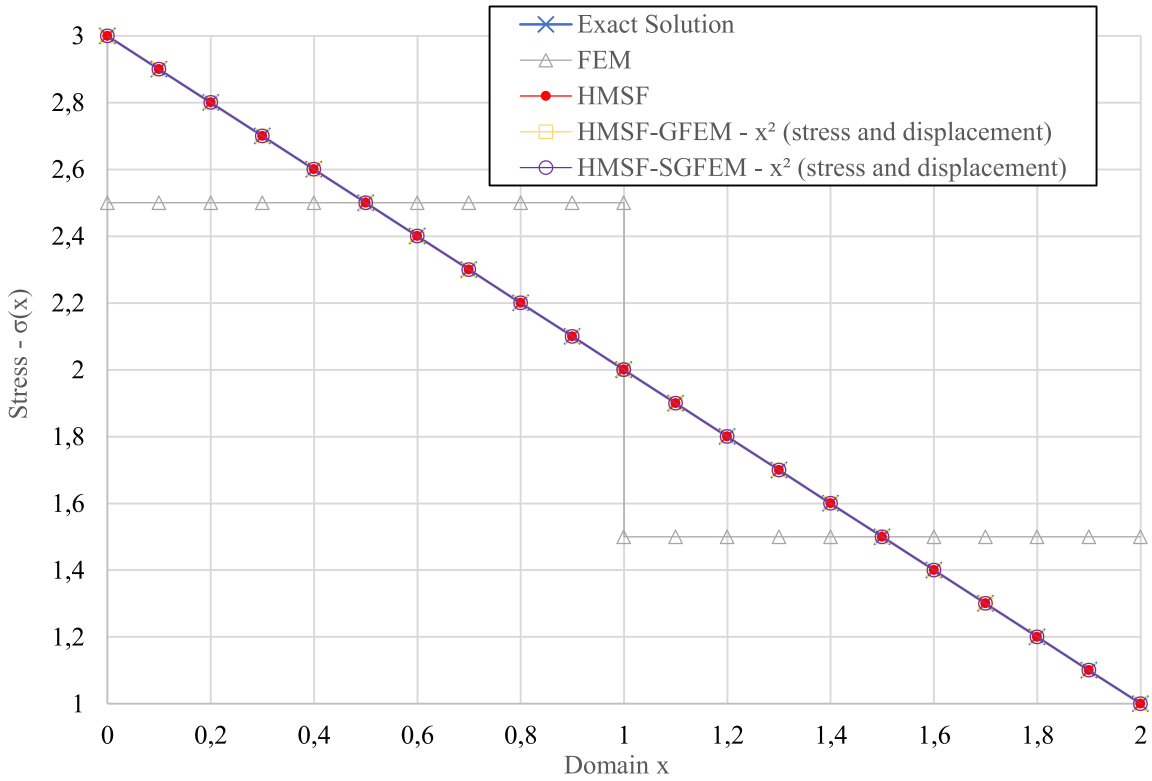

Source: own elaboration.

Due to the flexibility of the enrichment framework, the HMSF allows enrichment to be applied exclusively to the stress field. In this case, only the shape functions associated with the stress approximation are enriched, resulting in modifications to the terms of the submatrices defined in Eqs. (41) and (42).

This feature can be more readily understood from the strong-form formulation, represented by Eqs. (22) and (23), where the stress field and the displacement field appear as independent variables. Consequently, the approximation space of the stress field can be enhanced without altering the approximation adopted for the displacement field, providing additional flexibility in the construction of the numerical formulation.

It should be noted that when enrichment is applied exclusively to the **stress field** within the HMSF framework, the domain displacement matrix (Eq. (42)) is also affected. This modification is sufficient to improve the approximation of the displacement field, even though no direct enrichment is introduced into its interpolation space. Such behavior can be verified from the numerical results presented below.

The results obtained using the **HMSF-GFEM** and **HMSF-SGFEM** formulations with enrichment applied solely to the stress field are illustrated in Figures 15 and 16. These results demonstrate that stress-field enrichment not only enhances the representation of stresses but also leads to a significant improvement in the accuracy of the displacement field.

Figura 9 - Comparison of the displacement field in the domain obtained from the exact solution, FEM, HMSF, HMSF-GFEM, and HMSF-SGFEM, considering enrichment applied exclusively to the stress field.

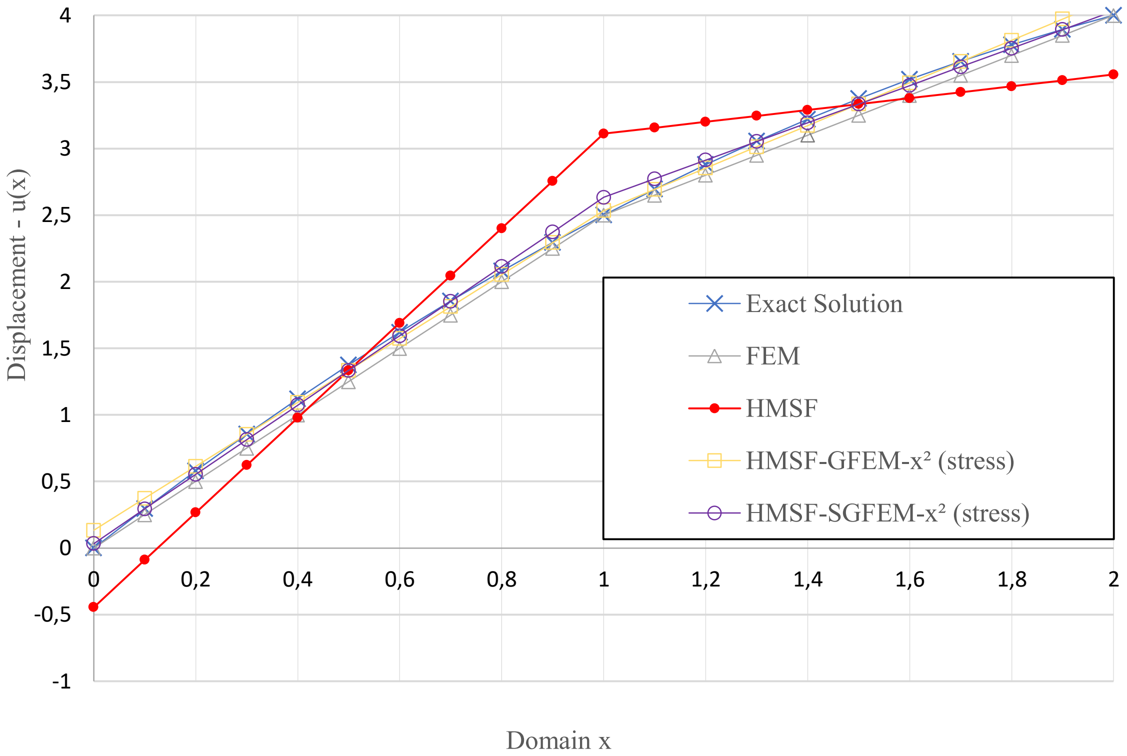

Source: own elaboration.

Figura 10 - Comparison of the stress field in the domain obtained from the exact solution, FEM, HMSF, HMSF-GFEM, and HMSF-SGFEM, considering enrichment applied exclusively to the stress field.

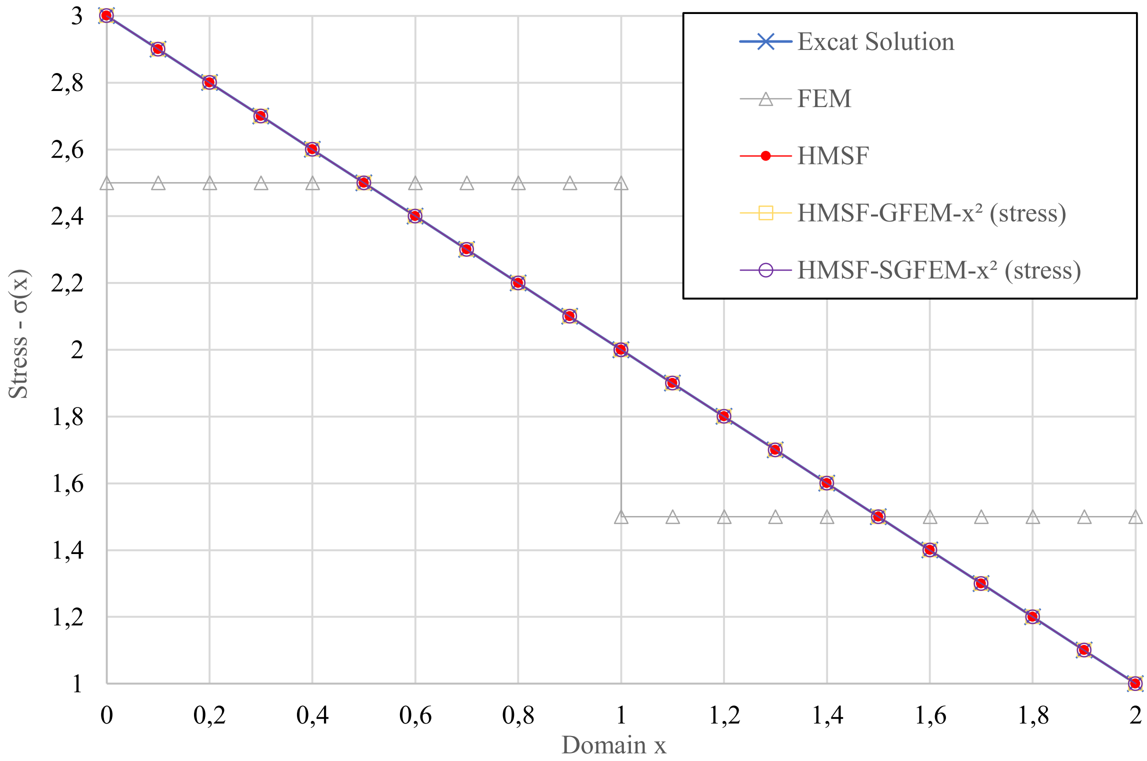

Source: own elaboration.

To quantitatively assess the accuracy of the numerical formulations, the normalized L_2-error, $\bar{e}_{L_2}$, defined by Eq. (70), is employed to evaluate the displacement field. The accuracy of the stress field is measured using the energy error, $\bar{e}_{energy}$, defined by Eq. (71). The corresponding results obtained for the different formulations are summarized in Table 3.

Table 3 - Comparison of errors between the methods presented.

Method	Error in displacement $\bar{e}_{L_2}$	Energy error $\bar{e}_{energy}$
FEM	3,50%	13,87%
HMSF	11,77%	0%
HMSF-GFEM – Enrichments applied to stress and displacement fields	0,75%	0%
HMSF-SGFEM – Enrichments applied to stress and displacement fields	1,12%	0%
HMSF-GFEM – Enrichment applied to the stress field	1,81%	0%
HMSF-SGFEM – Enrichment applied to the stress field	1,81%	0%

Source: own elaboration.

As expected, the enrichment procedures improved the accuracy of the displacement-field approximation while preserving the high-quality representation of the stress field. It is particularly noteworthy that, even when enrichment was applied exclusively to the stress field, a significant improvement was observed in the displacement approximation throughout the domain.

Another objective of this work is to assess the conditioning of the coefficient matrix resulting from the different formulations. To this end, the GFEM and SGFEM enrichment techniques were incorporated into the HMSF framework, and the corresponding condition numbers were evaluated. The conditioning results obtained for the various formulations are presented in Table 4.

Table 4 - Comparison of the condition numbers of the coefficient matrices associated with the different formulations.

Method	Conditioning
FEM	9
HMSF	2,73 E+8
HMSF-GFEM – Enrichments applied to stress and displacement fields	3,36 E+8
HMSF-SGFEM – Enrichments applied to stress and displacement fields	3,44 E+8
HMSF-GFEM – Enrichment applied to the stress field	17,15
HMSF-SGFEM – Enrichment applied to the stress field	30,85

Source: own elaboration.

It can be observed that the polynomial enrichment function x^2 adopted in this study produced no significant difference in the order of magnitude of the condition numbers associated with the HMSF-GFEM and HMSF-SGFEM coefficient matrices.

The analysis of the eigenvalues of the HMSF coefficient matrix, after the application of the boundary conditions, can be used as a complement to the **Inspection Test**. This additional analysis is important because, depending on the enriched fields and the enrichment functions employed, null eigenvalues—also referred to as **spurious modes**—may still be present in the system.

As previously discussed, the eigenvalues of the HMSF coefficient matrix possess a clear physical interpretation. Positive eigenvalues are associated with the domain stress parameters, $\mathbf{s}_{\Omega}$, whereas negative eigenvalues correspond to the displacement field. Zero eigenvalues, when present, represent spurious kinematic modes and are related to the displacement degrees of freedom, either in the domain or on the boundary, that is, $(\mathbf{q}_{\Omega} + \mathbf{q}_{\Gamma})$.

A comparison of the eigenvalue spectra obtained for the different formulations applied to the one-dimensional problem is presented in Table 5. This comparison provides additional insight into the stability and solvability characteristics of the enriched HMSF formulations.

Table 5 - Comparison of the eigenvalues obtained from the different formulations for the bar problem subjected to axial loading.

Methods	Eigenvalues		
	Positive	Negative	Zero
HMSF	3	3	1
HMSF-GFEM – Enrichments applied to stress and displacement fields	5	5	1
HMSF-SGFEM – Enrichments applied to stress and displacement fields	5	5	1
HMSF-GFEM – Enrichment applied to the stress field	5	4	0
HMSF-SGFEM – Enrichment applied to the stress field	5	4	0

Source: own elaboration.

Finally, it can be observed that the application of enrichment exclusively to the stress field, as expected, improves the displacement approximation while preserving the excellent accuracy and convergence properties of the stress field. In addition, this enrichment strategy leads to an improvement in the conditioning of the coefficient matrix and a reduction in the number of spurious kinematic modes.

The results also show that the conditions established by the **Inspection Test**, represented by Eqs. (83) and (84), are satisfied. For the case considered, these conditions, together with the eigenvalue analysis, indicate that the resulting enriched system is stable and solvable. Therefore, the existence of a valid numerical solution is ensured for the formulation under consideration.

CONCLUSIONS

This work investigated the application of the Hybrid-Mixed Stress Formulation (HMSF) combined with enrichment techniques based on the Generalized Finite Element Method (GFEM) and the Stable Generalized Finite Element Method (SGFEM). The objective was to evaluate the potential of these formulations to improve the approximation of displacement fields while preserving the excellent stress-field representation characteristic of the HMSF.

Initially, the HMSF was applied to a one-dimensional bar subjected to axial loading. The results demonstrated the ability of the formulation to accurately recover the stress field, reproducing the exact stress solution for the problem considered. However, although the stress approximation was highly accurate, the displacement field obtained through the HMSF exhibited lower accuracy than that obtained using the classical FEM.

To overcome this limitation, enrichment techniques based on GFEM and SGFEM were incorporated into the formulation. The results showed that both enrichment strategies improved the displacement approximation by locally increasing the approximation space without requiring mesh refinement. The improvements obtained in the displacement field were also reflected in the stress field, although the HMSF already exhibited excellent stress recovery capabilities.

The enriched formulations HMSF-GFEM and HMSF-SGFEM were then analyzed considering enrichment applied simultaneously to the stress and displacement fields, as well as enrichment applied exclusively to the stress field. In both cases, significant improvements were observed in the displacement approximation. Particularly noteworthy was the fact that enrichment restricted to the stress field was sufficient to improve displacement results while maintaining the high accuracy of the stress representation. This finding highlights the strong coupling between the variables in the HMSF framework and suggests that selective enrichment of the stress field may be an efficient strategy for improving overall solution quality.

The numerical conditioning of the resulting linear systems was also investigated. The analyses showed that the polynomial enrichment function adopted in this work, (x^2), did not produce significant differences in the order of magnitude of the condition numbers associated with the HMSF-GFEM and HMSF-SGFEM formulations. Nevertheless, the

SGFEM maintained the advantages associated with its construction, which aims to control conditioning problems commonly encountered in enriched formulations.

In addition, the Inspection Test and the eigenvalue analysis of the coefficient matrices were employed to evaluate the stability and solvability of the enriched formulations. The eigenvalue spectra confirmed the physical interpretation previously established for the HMSF, where positive eigenvalues are associated with stress parameters, negative eigenvalues are related to displacement variables, and zero eigenvalues correspond to spurious kinematic modes. The results demonstrated that selective enrichment of the stress field contributed to reducing the number of spurious modes while preserving the solvability conditions of the system.

Overall, the results indicate that the combination of HMSF with enrichment techniques constitutes a promising strategy for improving numerical approximations. In particular, the HMSF-SGFEM formulation combines the excellent stress recovery characteristics of the HMSF with enhanced displacement approximations and satisfactory numerical conditioning. The proposed approach therefore represents a viable alternative for the analysis of engineering problems in which accurate stress evaluation and robust numerical performance are required.

The authors hope that the findings presented herein will serve as a foundation for future investigations involving the extension of the proposed formulations to two- and three-dimensional problems, the development of alternative enrichment strategies, and the assessment of the method in more complex applications, such as stress concentration problems, material discontinuities, fracture mechanics, and topology optimization.

REPLICATION OF THE RESULTS

To promote reproducibility and facilitate future research, the algorithms implemented in this work, along with documentation describing their installation and execution, have been made publicly available in the following GitHub repository: https://github.com/wesleygois-ufabc/HMSF-HMSF-GEFM-and-HMSF-SGFEM-Applied-to-Axial-Bar-Problems.git.

ACKNOWLEDGEMENTS

This work was supported by the Coordination for the Improvement of Higher Education Personnel, CAPES, through a graduate scholarship for the second author. The authors are also thankful for the financial support of CNPq (National Council for Research and Development) under grant number 471291/2013-7.

AUTHOR CONTRIBUTIONS

Conceptualization, W Góis, Luis A P Navarro and Rafaela R Gomes; Methodology, W Góis, Edson da C Eduardo, José V de M Neto and Luis A P Navarro; Investigation, Rafaela R Gomes, S Hass and José V de M Neto; Writing - original draft W Góis and José V de M Neto; Writing - review & editing, W Góis; Funding acquisition, W Góis; Resources, W Góis; Supervision, W Góis.

DECLARATIONS

On behalf of all the authors, the corresponding author states that there are no conflicts of interest. The authors whose names are listed immediately below certify that they have no affiliations with or involvement in any organization or entity with any financial interest (such as honoraria; educational grants; participation in speakers' bureaus; membership, employment, consultancies, stock ownership, or other equity interest; and expert testimony or patent-licensing arrangements), or nonfinancial interest (such as personal or professional relationships, affiliations, knowledge or beliefs) in the subject matter or materials discussed in this manuscript. Author names: José Vieira de Melo Neto, Luis Armando Piccino Navarro, Edson da Costa Eduardo, Stefan Hass, Rafaela Rodrigues Gomes and Wesley Góis.

REFERENCES

Babuška, I., Caloz, G., Osborn, J. E. Special finite element method for a classe of second order elliptic problems with rough coefficients. **SIAM Journal on Numerical Analysis**, v.31, n.4, p. 727-981, 1994. DOI: https://doi.org/10.1137/0731051

Babuška, I., Melenk, J. M. The partition of unity method. **International Journal for Numerical Methods in Engineering**, v. 40, p. 727-758, 1997. DOI: http://dx.doi.org/10.1002/(SICI)1097-0207(19970228)40:4<727::AID-NME86>3.0.CO;2-N

DE Freitas, J. A. T.; DE Almeida, J. P. M.; Pereira, E. M. B. R. Non-conventional formulations for the finite element method. **Structural Engineering and Mechanics**, v. 4, n. 6, p. 655–678, 1996. DOI: https://doi.org/10.12989/SEM.1996.4.6.655

Duarte, C. A., Babuška, I., Oden, J. T. Generalized finite element methods for three-dimensional structural mechanics problems. **Computers & Structures**, 77(2), 215-232, 2000. DOI: https://doi.org/10.1016/S0045-7949(99)00211-4.

Duarte, C. A., Oden, J.T. Hp clouds – an hp meshless method. **Numerical Methods for Partial Differential Equations**. John Wiley & Sons, p. 1 – 34, 1996. DOI: https://doi.org/10.1002/(SICI)1098-2426(199611)12:6<673::AID-NUM3>3.0.CO;2-P.

Gois, W., Proenca, S. P. B. Generalized Finite Element Method on Nonconventional Hybrid-Mixed Formulation. **International Journal of Computational Methods**, 9(03), 1250038, 2012. DOI: http://dx.doi.org/10.1142/S0219876212500387.

Góis, W. Stress Hybrid and Hybrid-Mixed Finite Elements with Nodal Enrichment, PhD Thesis (in Portuguese), São Carlos School of Engineering, University of São Paulo. 2009.

Gupta, V., Duarte, C. A., Babuška, I., Banerjee, U. A stable and optimally convergent generalized FEM (SGFEM) for linear elastic fracture mechanics. **Computer Methods in Applied Mechanics and Engineering**, 266, 23-39, 2013. DOI: https://doi.org/10.1016/j.cma.2013.07.010.

The MathWorks Inc. (2022). MATLAB version: 9.13.0 (R2022b), Natick, Massachusetts: The MathWorks Inc. https://www.mathworks.com

Neto, J. V. M., Góis, W., Lins, R. Application of the Hybrid-Mixed Finite Element Method with Stabilized Nodal Enrichment on 2D Problems. 2022. DOI: 10.26678/ABCM.MECSOL2022.MSL22-0203.

Oden, J. T., Duarte, C.A., Zienkiewicz, O. C. A new cloud – based hp finite element method. **Computer Methods in Applied Mechanics and Engineering**, v. 153, p. 117-126, 1998. DOI: https://doi.org/10.1016/S0045-7825(97)00039-X.

SMATH LLC. SMath Studio. Versão 1.3. Santo André: SMath LLC, 2025.

Strouboulis, T.; Babuška, I.; Copps, K. The design and analysis of the Generalized Finite Element Method. **Computer Methods in Applied Mechanics and Engineering**, v. 181, n. 1, p. 43–69, 2000. DOI: https://doi.org/10.1016/S0045-7825(99)00072-9.

Zienkiewicz, O. C., S. Qu, R. L. Taylor, S. Nakazawa. The patch test for mixed formulation. **International Journal for Numerical Methods in Engineering**, v.23, p. 1873-1882, 1986. DOI: https://doi.org/10.1002/nme.1620231007 .